ELECTROMAGNETIC DECAY OF FRAGMENTED ANALOGUE STATES IN ^{55}MN AND ^{59}CO

by

William Carter Peters

Department of Physics
Duke University

Date: _____

Approved:

_____
E. G. Bilpuch, Supervisor

_____

_____

_____

_____

A dissertation submitted in partial fulfillment of the requirements for the degree of Doctor of Philosophy in the Department of Physics in the Graduate School of Arts and Sciences of Duke University

1972

ABSTRACT

(Physics)

ELECTROMAGNETIC DECAY OF FRAGMENTED ANALOGUE STATES IN ^{55}MN AND ^{59}CO

by

William Carter Peters

Department of Physics
Duke University

Date: _____

Approved:

_____
E. G. Bilpuch, Supervisor

_____

_____

_____

_____

An abstract of a dissertation submitted in partial fulfillment of the requirements for the degree of Doctor of Philosophy in the Department of Physics in the Graduate School of Arts and Sciences of Duke University

1972

ELECTROMAGNETIC DECAY OF FRAGMENTED ANALOGUE STATES IN ^{55}MN AND ^{59}CO

by

William Carter Peters

The inelastic and gamma decay of the fragmented analogues of the ground states of ^{55}Cr and ^{59}Fe has been studied. Using the TUNL high resolution electrostatic analyzer-homogenizer system, the ^{54}Cr(p,γ) excitation function from 1.98 to 2.02 MeV and the ^{58}Fe(p, γ) excitation function from 2.15 to 2.30 MeV were measured with a 7.6 cm by 7.6 cm NaI(Tl) detector. The over-all proton energy resolution was ~ 350 eV. Using an 80 cm^3 Ge(Li) detector at 55^o with respect to the incident beam, absolute inelastic proton and gamma decay widths were measured for 10 resonances in the vicinity of the ground state analogue in ^{55}Mn and for 22 resonances in the vicinity of the ground state analogue in ^{59}Co. The elastic proton widths and spins for these resonances had been previously determined in high resolution proton elastic scattering experiments.

Eight of the resonances in ^{55}Mn and ten of the resonances in ^{59}Co were identified as fragments of the respective ground state analogues.

Absolute gamma decay widths for transitions from these fragments to the corresponding antianalogue states were found to be weak. The M1 strengths of both of these transitions, assuming no E2 admixtures, were 0.05 Weisskopf units, in agreement with results for non-fragmented analogue states in this mass region. Comparisons of the gamma decay of the ground state analogue with the beta decay of the ground states of ^{55}Cr and ^{59}Fe were made. In general, the widths corresponding to the beta decay were weaker than the experimentally determined gamma decay widths. The best agreement between the beta decay and gamma decay widths occurred for the transitions to the ground state of ^{55}Mn.

The inelastic proton and gamma decay widths were examined for possible correlations with the enhanced elastic channel widths. Positive correlations which were significant at a confidence level of greater than 95% were measured between the elastic and inelastic widths for both analogue states, between the elastic and ground state transition widths for the ground state analogue in ^{55}Mn, and between the elastic and total capture widths for the ground state analogue in ^{59}Co. The correlations of channel widths for resonances in ^{59}Co not associated with the ground state analogue were consistent with purely statistical behavior.

ACKNOWLEDGMENTS

I would like to express my gratitude to my advisor, Dr. E. G. Bilpuch, for his guidance and encouragement during the course of these experiments. Special thanks also to Dr. G. E. Mitchell for his advice and suggestions throughout these experiments and in particular in the preparation of this dissertation.

I am indebted to Dr. J. C. Browne, Dr. J. D. Moses, Dr. D. P. Lindstrom, Dr. N. H. Prochnow and especially to Dr. G. L. Morgan for their helpful discussions and significant contributions to my research. Thanks are also due W. Wilson, D. Flynn and F. Wimpey for help in taking some of the data.

The assistance of Mr. Sidney Edwards, Mr. Robert Rummel, Mr. Malcolm Smith and Mr. A. W. Lovette in constructing and maintaining the equipment used in these experiments is gratefully acknowledged. The many hours contributed by Mrs. Joseph Bailey and Mr. Al Rade in the preparation of the figures in this dissertation is sincerely appreciated. I would also like to thank Mrs. Jean Luffman for typing this dissertation.

Discussions with Dr. L. C. Biedenharn over several years have contributed significantly to this research. Special thanks are extended to Dr. A. M. Lane for his correspondence and advice on several aspects of this work.

Finally, I would like to thank my wife, Nancy, for her encouragement and understanding during these past five years.

This work was supported in part by the U. S. Atomic Energy Commission. Some data analysis was performed at the Triangle Universities Computational Center, which is supported in part by the National Science Foundation.

W. C. P.

CONTENTS

LIST OF FIGURES

LIST OF TABLES

ELECTROMAGNETIC DECAY OF FRAGMENTED ANALOGUE STATES IN ^{55}MN AND ^{59}CO

Chapter I

INTRODUCTION

In 1961 Anderson, Wong and McClure presented the first results of a series of experiments which established isobaric analogue states (IAS) in medium weight nuclei. In the time-of-flight spectra for (p,n) reactions on a number of nuclei in the mass range 50 to 90, very strong neutron groups were observed. The reaction was interpreted as a simple charge exchange mechanism which populated the isobaric analogue of the ground state of the target. Previously it had been assumed that analogue states would only exist in light elements since large Coulomb effects were expected to destroy the usefulness of isospin as a good quantum number. Anderson's work, therefore, opened a new era for analogue state experiments and increased interest in isospin.

An even more important development occurred in 1964 when Fox, Moore and Robson discovered that analogue states (rather high in excitation energy) could be populated in elastic proton scattering on medium and heavy nuclei. Later in the same year the existence of fine struc-

ture (fragmentation of the analogue state into many components) was indicated (Richard et al., 1964). In this experiment the total energy resolution (about 3 keV) was inadequate to completely resolve the fine structure components. In 1965 Keyworth, Kyker, Bilpuch and Newson, using an electrostatic analyzer-homogenizer system (Parks et al., 1958) and a windowless cryogenic gas target chamber (Parks et al., 1964), succeeded in resolving the fine structure of analogue states populated in $^{40}A(p,p)^{40}A$. In this experiment the Duke group achieved a total energy resolution on the order of 200 eV. The fine structure consisted of many compound nuclear resonances whose spin and parity were the same as that of the analogue state. The enhancement of these states was interpreted as the result of mixing between the analogue and ordinary compound nuclear states. Subsequently the high resolution group at Duke found that solid targets only slightly affected the total energy resolution (Browne et al., 1969). Since then the fine structure of analogue states has been systematically explored in the mass 40-60 region (Browne, 1969 ; Moses, 1970; Lindstrom, 1970; Prochnow, 1971; and Wilson, 1972).

The electromagnetic decay of analogue states has also proved to be very interesting. Some of the earliest and most significant studies were performed by Endt (1964). Endt observed that in the s-d shell the gamma decay from the analogue proceeded predominantly to a single bound state with the same spin and parity as the analogue. These special states were later called "anti-analogue states" (AIAS). The AIAS were described as

consisting of admixtures of the same particle-core components as the analogue state, but with different (isospin dependent) weights so that the two states are orthogonal. Such simple, strong IAS to AIAS transitions were not observed in the decay of $p_{3/2}$ analogues in the mass 40 to 60 region. The (^{3}He,d) spectroscopic factors indicated that the antianalogue states were fragmented. Even more importantly, the IAS-AIAS M1 transition strength was reduced by factors of 10 to 1000. Maripuu (1970C) and Hirata (1970) attempted to explain this hindrance in terms of core polarization effects. Recent experiments on $g_{9/2}$ analogues in the Ni isotopes (Fodor et al., 1970; Szentpetery et al., 1972; Maripuu et al., 1972) indicate that the analogue-antianalogue strengths are again large.

The fragmentation of the analogue states complicated the gamma decay studies. Some of the earliest work on the gamma decay of fine structure fragments was performed by Chasman et al. (1967). They studied the gamma decay of an analogue state in ^{38}A which consisted of only two fragments (Erne et al., 1966). The decays of the two fragments were observed to be similar and were dominated by strong IAS-AIAS transitions typical of the s-d shell. Several experiments in the f-p shell (see Table 2 in Chapter II for references) demonstrated that the decay of the fragments of analogue states in this region exhibit rather weak antianalogue effects consistent with the decay of non-fragmented analogue states.

A recent area of interest has been correlations between fine structure channel decay widths. Lane (1969) has given a comprehensive treatment of fine structure and channel correlations. Preliminary experi-

mental results (Vingiani et al., 1968B; Vingiani et al., 1971A) indicate correlations between total gamma widths and the corresponding elastic proton widths.

This dissertation describes experiments undertaken to study the electromagnetic decay of the highly fragmented analogues of the ground states of ^{55}Cr (8 fragments in ^{55}Mn) and ^{59}Fe (10 fragments in ^{59}Co). The objectives of the experiments were threefold. First, since almost no electromagnetic decay studies have been made on highly fragmented analogue states, it was desired to know if the fragments decay the same way. Secondly, $^{54}Cr(p,\gamma)\,^{55}Mn$ and to a lesser extent $^{58}Fe(p,\gamma)^{59}Co$ offered the opportunity to compare the gamma decay of the ground state analogue with the beta decay of the corresponding parent (the ground states of ^{55}Cr and ^{59}Fe). In recent years similar comparisons have been made for several non-fragmented analogues. A survey of these has been given by Hanna (1969). The third reason for this work was to determine if any correlations exist between exit channel widths. According to Lane, such correlations would be expected where both channels were enhanced by the analogue state. Comparisons have been made between the elastic proton widths previously measured by Moses (1970) and Lindstrom (1970), partial gamma decay widths for transitions from the analogue to low-lying levels, total capture widths estimated from secondary transitions, and inelastic proton widths determined from the yield of the gamma rays associated with the inelastic decay.

The measurements made in these experiments consist of NaI(Tl) yield curves over the regions of the analogue states and absolute gamma decay widths for transitions from each of the fragments of the analogue that were resolved in the elastic scattering work. The NaI(Tl) yield curves were obtained with a 7.6 cm by 7.6 cm detector placed 7.6 cm from the targets at an angle of 90° with respect to the incident beam. The decay widths were measured with an 80 cm^3 Ge(Li) detector located 5 cm from the targets at an angle of 125° with respect to the beam. The absolute efficiency of the Ge(Li) detector was measured in order to determine the absolute widths.

In Chapter II a general background is given concerning anti-analogue states, IAS-AIAS M1 transition rates, beta decay and statistical properties of reaction widths and analysis. Chapter III describes the experimental equipment and procedure. The experimental results and analysis of these data are presented in Chapters IV and V, followed by a brief summary in Chapter VI.

Chapter II

GENERAL BACKGROUND

The analysis of the electromagnetic decay of the analogue states described in this dissertation requires a consideration of several different topics in nuclear physics. One of these is the concept of an antianalogue state. This concept originated from some of the earliest proton capture studies. Another topic of interest is the general treatment of M1 transition rates, particularly those corresponding to $\Delta T = 1$ (where T is the isospin quantum number) transitions. Decay from an IAS to the corresponding AIAS is predominantly such a transition. A third topic due consideration is Gamow-Teller beta decay. Since the isovector components of the electromagnetic M1 operator and the beta decay operator are very similar, a comparison can be made between the beta decay of the parent state and the electromagnetic transition from the analogue to the same final state. In order to make some of the quantitative comparisons between various sets of widths measured in this experiment, a number of statistical considerations are necessary. In particular, the statistical distributions from which the partial and total decay widths come are important to the esti-

mate of the statistical significance (confidence factor) of the correlation coefficients determined from the experimental data. Due to the broad scope of these topics it is impractical to present a comprehensive treatment of them. Only those results directly relevant to this dissertation will be discussed here.

A. Antianalogue States

The concept of an antianalogue state is fairly new. Its origin can apparently be traced back only to 1966. At a symposium on research in the s-d shell, the results of some of the first capture experiments on analogue states were reported (Endt, 1966). In ^{35}Cl, ^{31}P and ^{27}Al, the electromagnetic decay of the IAS was observed to proceed to a state with the same spin and parity as the analogue. The transitions were predominantly M1 with strengths on the order of several Weisskopf units (for M1 transitions, 1 Wu = 0.021 E_γ^3 eV, where E_γ is the energy of the emitted gamma ray in MeV). Later capture experiments in the s-d shell yielded similar results: strong gamma transitions with simple decay patterns (usually only one strong transition, for example, Endt, 1969).

The earliest explanation for the unusual s-d shell IAS decay was fairly simple. In coupling a proton (whose isospin is $\bar{t} = \overline{1/2}$, $t_z = -1/2$) in an orbit (ℓ, j) to an even-even core whose isospin is T_o, two states with the same spin and parity are obtained. One is a state with

isospin $T_> = T_o + 1/2$, the analogue state. The other, a state whose isospin is $T_< = T_o - 1/2$, is the antianalogue. According to this early interpretation, states which resemble each other so much would be expected to be connected by relatively large M1 matrix elements. Hence the strength of M1 transitions from the IAS was assumed to be concentrated in the AIAS transition. In Fig. 1 the relationship between the parent, analogue, and antianalogue states is shown. At the top, the parent state is schematically illustrated. The parent state is assumed to consist of closed proton and neutron shells (only one neutron orbit is above the closed proton shell) with one excess neutron in an orbit outside the core. The isospin lowering operator, T^-, acting on the parent state then yields the analogue state, as shown in the middle of the drawing. The antianalogue state, shown at the bottom of Fig. 1, is a state which has the same shell model configuration as the analogue state but with different weights. The analogue and antianalogue states are orthogonal.

After the initial success of this simple explanation, difficulties with this description of IAS-AIAS decay began to occur (Endt, 1968). In the f-p shell the gamma decay of analogue states was not nearly as simple as that in lighter nuclei. The IAS to AIAS M1 strengths were typically inhibited by factors on the order of 10 to 1000 with the stronger transitions often not even proceeding to the antianalogue states. Later capture experiments have shown that these complications occur systematically throughout the f-p shell.

Figure 1. Diagram of the relationship between the parent, analogue, and antianalogue states.

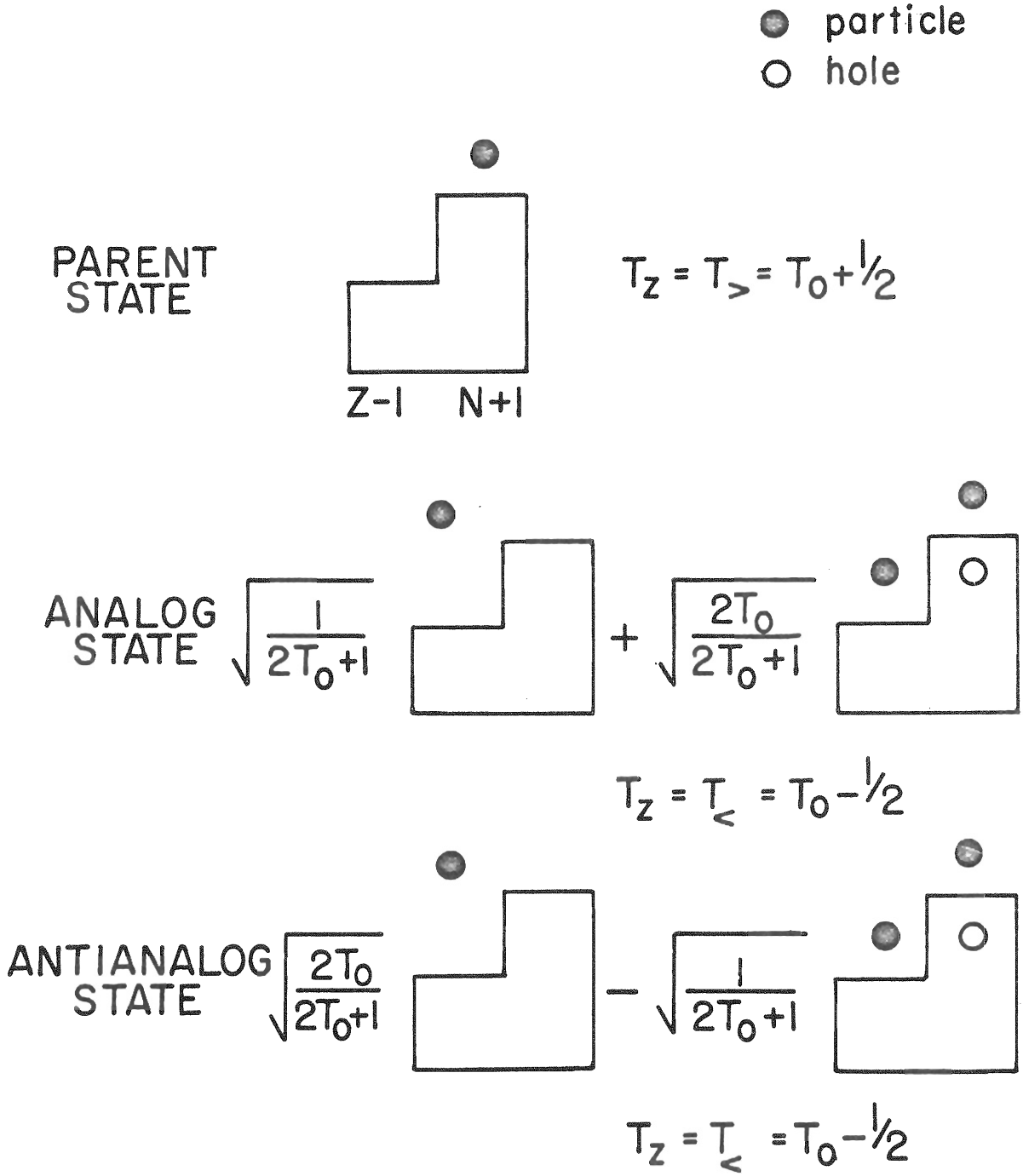
particle
hole
PARENT STATE
Z-1 N+1
$T_z = T_> = T_0 + 1/2$
ANALOG STATE
$\sqrt{\frac{1}{2T_0+1}}$
+
$\sqrt{\frac{2T_0}{2T_0+1}}$
$T_z = T_< = T_0 - 1/2$
ANTIANALOG STATE
$\sqrt{\frac{2T_0}{2T_0+1}}$
−
$\sqrt{\frac{1}{2T_0+1}}$
$T_z = T_< = T_0 - 1/2$

The explanation for the apparent anomalous gamma decay in the f-p shell is still not completely clear. Several attempts have been made to explain the inhibition of the M1 transition strengths within the framework of the shell model. Some of these will be discussed in the next section. Part of the additional complexity of the decay of IAS in this region is due to fragmentation of the antianalogue by the strong nuclear interaction. This splitting would be expected to be on the order of a few MeV. Experimentally there is evidence for such splitting. In particular, (^{3}He,d) experiments in this mass region have found spectroscopic strengths to be spread among several levels rather than concentrated primarily in one. Robson (1969) has pointed out that the definition of antianalogue states, particularly in heavier nuclei, is somewhat vague. When there is more than one closed neutron orbit above the closed proton shell, more than one state exists which is orthogonal to the analogue and has the same quantum numbers (J^π, $T_<$ etc.). For n neutron orbits above the closed proton shell there are n - 1 mutually orthogonal states which can be considered to be antianalogues.

B. M1 Transition Rates

The theory of electric and magnetic multipole transitions yields several important selection rules for electromagnetic transitions between nuclear levels. Some of these have been summarized by Warburton (1966).

There are two selection rules in particular which have been of considerable importance to the experiments described in this dissertation, namely,

I. M1 transitions from $J = L + 1/2$ levels can be expected to be stronger by a factor of 10 or more than from $J = L - 1/2$ (with $L \neq 0$) levels.

II. $J \rightarrow J$ M1 transitions are expected to be favored over similar transitions for which $\Delta J = 1$.

Rule II has been called "Erne's Rule" (Endt, 1967). A derivation of these selection rules has been given by Talmi and Unna (1960). Some of the results given by them are the following:

1. The radiative width for an M1 transition between an initial state $|\alpha T J\rangle$ and a final state $|\alpha' T' J'\rangle$ is

$$\Gamma_\gamma(M1) = 2.76 \times 10^{-3} E_\gamma^3 \Lambda(M1) \text{ eV}$$

where E_γ is the energy of the emitted gamma ray in MeV and

$$\Lambda(M1) = (\alpha T J \| \Omega(M1) \| \alpha' T' J')^2/(2J+1)$$

is called the "transition strength". The reduction in this matrix element has not been carried out over the isospin projection. The M1 operator is

$$\Omega(M1) = B \sum_i (g_\ell \ell + g_s s)_i , \qquad \text{with } B = \frac{eh}{2mc} \sqrt{\frac{3}{4\pi}}$$

which is summed over all i particles. Similar radiative widths for E1 and E2 transitions are

$$\Gamma_\gamma(E1) = 2.5 \times 10^{-1} E_\gamma^{\,3} \Lambda(E1)\ eV$$

and

$$\Gamma_\gamma(E2) = 8.0 \times 10^{-6} E_\gamma^{\,5} \Lambda(E2)\ eV\ .$$

2. In pure jj coupling the magnetic dipole operator

$$\Omega(M1) = B \sum_i (g_\ell\, \ell + g_s s)_i$$

where for protons $g_\ell = 1$, $g_s = 2 \times 2.793$, and for neutrons $g_\ell = 0$ and $g_s = 2 \times (-1.914)$, can be written as

$$\Omega(M1) = B \sum_i \left[\frac{1}{2}(1 - t_{3i}) g_j^p + \frac{1}{2}(1 + t_{3i}) g_j^n\right] j_i$$

with t_{3i} being the third component of the isospin and g_j the g factor for the corresponding particle in the j_i orbit. These g factors are given by the Schmidt values

$$g_j = (g_\ell + \tfrac{1}{2} g_s)/j \quad \text{for} \quad j = \ell + \tfrac{1}{2}$$

and

$$g_j = \left[g_\ell(\ell + 1) - \tfrac{1}{2} g_s\right] /(j + 1) \text{ for } j = \ell - \tfrac{1}{2}\ .$$

From these equations and the expressions for the M1 radiative width, it follows that for $\Delta T = 1$ transitions

$$\Gamma_\gamma(M1) \propto (g_j^p - g_j^n)^2\ .$$

Using the Schmidt values for the g factor term gives

$$\Gamma_\gamma(M1) \propto (\ell + 4.71)^2/(\ell + \tfrac{1}{2})^2 \text{ for } j = \ell + \tfrac{1}{2}$$

and

$$\Gamma\ (M1) \propto (\ell - 3.71)^2/(\ell + \tfrac{1}{2})^2 \text{ for } j = \ell - \tfrac{1}{2}\ .$$

Selection rule I given at the beginning of this section is based upon these equations. For example, for $\ell = 1, 2,$ and 3 the $\ell + \frac{1}{2}$ to $\ell - \frac{1}{2}$ ratios are 4.5, 15.4 and 117, respectively. For $\Delta T = 0$ M1 transitions the radiative width is proportional to $(g_j^p + g_j^n)^2$.

3. The magnetic dipole operator can be written (for example, Maripuu, 1969) as $\Omega(M1) = \Omega_o(M1) + \Omega_1(M1)$, where

$$\Omega_o(M1) = B \sum_i \left[\frac{g_j^p + g_j^n}{2}\right] j$$

and

$$\Omega_1(M1) = -B \sum_i \left[\frac{g_j^p - g_j^n}{2}\right] j \times t\ .$$

Then reduction of the transition strength matrix element in isospin space gives

$$\Lambda(M1) = \left[\langle T\, T_z\ 0\ 0 \mid T'\ T_z\rangle \langle J'\ T' \| \Omega_o(M1) \| J\ T\rangle + \langle T\, T_z\ 1\ 0 \mid T'\ T_z\rangle \langle J'\ T' \| \Omega_1(M1) \| J\ T\rangle\right]^2 \Big/ \left[(2J+1)\sqrt{2T'+1}\right]\ .$$

The first term in the parenthesis is a scalar and the second a vector in isospin space; they are thus referred to as the isoscalar and isovector components. The isoscalar matrix element must be zero between states having different isospin. Hence for IAS decay to

ordinary $T_<$ states only the isovector component will contribute. For example, Watson et al. (1967) have calculated the "M1 transition speed" between IAS and AIAS in ^{35}Cl. They expand a $J_o = 0$, $T_o = 1$, $A = 34$ core coupled to an extracore nucleon by a Clebsch-Gordan expansion to obtain

$$\left|{}^{35}\mathrm{Cl}\ 3/2\ 1/2\right\rangle = (1/3)^{1/2}\left|{}^{34}\mathrm{S}+\mathrm{p}\right\rangle + (2/3)^{1/2}\left|{}^{34}\mathrm{Cl}+\mathrm{n}\right\rangle$$

for the analogue, and

$$\left|{}^{35}\mathrm{Cl}\ 1/2\ 1/2\right\rangle = (2/3)^{1/2}\left|{}^{34}\mathrm{S}+\mathrm{p}\right\rangle - (1/3)^{1/2}\left|{}^{34}\mathrm{Cl}+\mathrm{n}\right\rangle$$

for the corresponding antianalogue. Then using the isovector part of the M1 operator and assuming no core transition gives for the M1 decay width, in Weisskopf units,

$$\Gamma_\gamma(\mathrm{M1}) = 0.13\, J(J+1)\,(g^p - g^n)^2\,(2T_o)/(2T_o+1)^2 \quad .$$

As shown in Table 1, this result agrees fairly well with the experimental values (Watson et al., 1967).

Table 1. Comparisons of M1 Transition Rates in ^{35}Cl

$E_>$ (MeV)	$E_<$ (MeV)	J^π	$(g^n - g^p)^2$	$\Gamma_\gamma(\mathrm{M1})$	$\Gamma_\gamma(\mathrm{M1})_{exp}$
7.84	4.17	$3/2^-$	14.5	1.6 Wu	1.0 Wu
7.54	3.16	$7/2^-$	4.85	2.2 Wu	1.6 Wu

4. Talmi and Unna have calculated the $\Delta T=1$ M1 transition strength for a two-nucleon configuration of a self-conjugate nucleus to be

$$\Lambda(M1)=\frac{2J'+1}{4}\left[\sqrt{j_1(j_1+1)(2j_1+1)}\begin{Bmatrix} j_1 & J & j_2 \\ J' & j_1 & 1 \end{Bmatrix}(g^n_{j1}-g^p_{j1})\right.$$

$$\left.+(-1)^{J+J'}\sqrt{j_2(j_2+1)(2j_2+1)}\begin{Bmatrix} j_2 & J & j_1 \\ J' & j_2 & 1 \end{Bmatrix}(g^n_{j2}-g^p_{j2})\right]^2$$

The J - J selection rule (II) follows from expressions such as these because of properties of the 6-j coefficients. The expression for $\Delta T = 0$ transitions contains the same coefficients.

The inhibition of IAS-AIAS M1 transitions in the f-p shell by factors on the order of 10 to 1000 has already been mentioned. In Table 2 a brief summary is given of (p,γ) experiments in this mass region whose results have included absolute decay width measurements. The column headed $\Gamma_\gamma(M1)$ is the sum of the widths for all transitions which conceivably could be M1 (for example, it includes transitions to all levels whose spin and parity is unknown). The next column, $\Gamma_a(\bar{A})$, is the sum of the widths for all transitions to potential AIAS, that is, transitions to all levels for which at least the ℓ value is known and which possibly have the same spin as the analogue. The last column, $\Gamma_b(\bar{A})$, is the strength of the transitionto the state with the same J as the IAS which has the largest (^{3}He,d)

Table 2. Survey of (p, γ) Experiments in the f-p Shell Populating Analogue States

Nucleus	E_{ex}(MeV)	J^{π}	$T_>$	Parent State (MeV)	E_p (MeV)	Γ_γ(M1) (Wu)	$\Gamma_a(\bar{A})$ (Wu)	$\Gamma_b(\bar{A})$ (Wu)	Ref.
^{55}Co	6.83	$3/2^-$	3/2	2.050	1.803 (1)	0.375	0.235	0.089	a
^{55}Co	6.92	$5/2^-$	3/2	2.140	1.887 (1)	0.136	0.040		a
^{57}Co	7.26	$3/2^-$	5/2	0.014	1.25 (3)	0.212	0.076	0.026	b
^{57}Co	7.64	$3/2^-$	5/2	0.367	1.65 (4)	0.385	0.100	0.066	b
^{51}Mn	6.31	$3/2^-$	3/2	1.899	1.059 (1)	0.090	0.033	0.018	c
^{53}Mn	7.55	$1/2^-$	5/2	0.560	1.006 (1)	0.450	0.080	0.040	d
^{43}Sc	6.14	$3/2^-$	3/2	2.048	1.242 (1)	0.159		0.020	e
^{47}Sc	6.69	$1/2^-$	3/2	2.607	1.81 (3)	0.309			e
^{49}Sc	10.30	$3/2^-$	7/2	2.016	1.86 (6)				f
^{49}Sc	11.55	$3/2^-$	9/2	0	1.97 (6)			< 0.0006	g
^{49}V	7.75	$3/2^-$	5/2	1.380	1.00 (2)	0.668	0.292	0.018	h
^{49}V	8.09	$1/2^-$	5/2	1.720	1.362 (1)	0.542	0.129		h
^{51}V	9.40	$3/2^-$	7/2	0	1.37 (3)	0.784	0.100	0.007	h

a. Martin et al., 1972.
b. Leslie et al., 1972.
c. Klapdor, 1971B.
d. Maripuu, 1970A.
e. Walinga et al., 1969.
f. Vingiani et al., 1971.
g. Vingiani et al., 1968A,B; Chilosi et al., 1968.
h. Maripuu, 1970B

spectroscopic factor. The Γ_b have been taken from Klapdor (1971A). The claim that the IAS-AIAS M1 transitions in the f-p shell are inhibited is based upon the Γ_b values. In order to determine the M1 strengths $\Gamma_\gamma(M1)$, $\Gamma_a(\bar{A})$, and $\Gamma_b(\bar{A})$, the E2/M1 mixing ratios (when unknown) were assumed to be small.

Several attempts have been made to explain the reduction in the IAS-AIAS M1 strength in the f-p shell. Maripuu (1970) has attributed the hindrance to core polarization effects, that is, to mixing of the antianalogue with states formed by coupling a valence nucleon to a core which is assumed to consist of a doubly closed inert part and an even number of active nucleons. M. Hirata (1970) has explained the effect in ^{49}Sc by introducing the "charge-exchange spin-flip collective mode", that is, by postulating the existence of a "charge-exchange spin-flip collective state" rather high in excitation energy which, he shows, will strongly absorb the M1 strength. Klapdor's summary (1971A) of work in the f-p shell notes that the hindrance of the IAS-AIAS M1 transitions appears to be an effect of the $f_{7/2}$ proton shell. Part of the basis for this claim is that I. Fodor et al. (1970), I. Szentpetery and J. Szucs (1972), and S. Maripuu et al. (1972) have shown that M1 transitions for $g_{9/2}$ IAS with the $f_{7/2}$ shell filled (specifically, in ^{59}Cu, ^{61}Cu, ^{63}Cu, ^{65}Ga, and ^{67}Ga) appear to again be of the order of Weisskopf units.

C. Beta Decay

In some cases it is possible to compare the beta decay of a parent state with the gamma decay of the corresponding analogue. Hanna (1969) has given an explicit formula (first derived by Kurath, 1965) for the relationship between the electromagnetic M1 transition strength $\Lambda(M1)$ and the beta decay strength $\Lambda(GT)$ for $\Delta T = 1$ transitions. In Hanna's notation, where $|f\rangle$ denotes the final and $|i\rangle$ the initial states involved in the transition,

$$\Lambda(M1) = 11.1 \frac{(CG)_\gamma^2}{(CG)_\beta^2} \left[1 + 0.11 \frac{\langle f \,|\ell t|\, i \rangle}{\langle f \,|st|\, i \rangle} \right]^2 \Lambda(GT) \quad .$$

The Clebsch-Gordan coefficients in this equation are

$$(CG)_\gamma = (T'_\gamma \; T'_{z\gamma} \; 1 \; 0 \;|\; T_\gamma \; T_{z\gamma})$$

and

$$(CG)_\beta = (T'_\beta \; T'_{z\beta} \; 1 \; 1 \;|\; T_\beta \; T_{z\beta}) \quad .$$

The ratio for the square of these coefficients for gamma decay and beta decay between the same isospin states is simply $1/T$. The matrix elements in the brackets are just those from the isovector component of the M1 operator discussed in section B. Assuming that the orbital matrix element is smaller than the spin matrix element, the matrix elements can be ignored to a fairly good approximation. This assumption is reasonable for $\Delta j = 1$ transitions, but presumably will be only a very rough estimate for $j \rightarrow j$ transitions. Conventionally, the beta decay transition strength

Table 3. Survey of Beta Decay-Gamma Decay Comparisons for Medium Weight Nuclei

Parent Nucleus	Transition J^{π}, T	Energy Transition (MeV)	Γ_{γ}(M1) (eV)	log ft	Γ_{β}(GT) (eV)	Reference
^{32}Si	$0^+,2 \rightarrow 1^+,1$	5.07 → 0.00	0.14	9.5	5×10^{-6}	Adelberger, Balamuth, 1971
^{49}Ca	$\frac{3}{2}^-,\frac{9}{2} \rightarrow \frac{3}{2}^-,\frac{7}{2}$	11.6 → 3.1	0.022	4.9	0.2	Mann, Bloom, 1970
			0.013	5.1	0.16	Maripuu, 1970
^{51}Ti	$\frac{3}{2}^-,\frac{7}{2} \rightarrow \frac{5}{2}^-,\frac{5}{2}$	9.4 → 0.32	0.74	4.8	0.43	Gaarde et al., 1970
	$\frac{3}{2}^-,\frac{7}{2} \rightarrow \frac{3}{2}^-,\frac{5}{2}$	9.4 → 0.93	0.012	5.4	0.08	
^{56}Mn	$3^+,3 \rightarrow 2^+,2$	11.5 → 0.846	0.021	7.4	0.0022	Sakai and Gehringer, 1970
	$3^+,3 \rightarrow 2^+,2$	11.5 → 2.658	0.056	5.6	0.078	
	$3^+,3 \rightarrow 2^+,2$	11.5 → 2.96	0.158	5.4	0.112	
	$3^+,3 \rightarrow 2^+,2$	11.5 → 3.37	0.193	5.1	0.193*	
	$1^+,3 \rightarrow 0^+,2$	11.6 → 0.00	0.702	5.0	0.702*	
	$1^+,3 \rightarrow 2^+,2$	11.6 → 0.846	0.33	5.7	0.11	
	$1^+,3 \rightarrow 2^+,2$	11.6 → 2.658	0.0098	6.2	0.02	

* These values were assumed in order to compute the absolute widths for the remaining transitions in the group. Sakai gave only relative widths.

is expressed in terms of the ft value. The relationship between this and $\Lambda(GT)$ is

$$ft = 4390/\Lambda(GT) \quad \text{(Hanna, 1969).}$$

The corresponding relationship between $\Gamma_\gamma(M1)$ and $\Lambda(M1)$ has been given in section B.

Several comparisons of the gamma decay of an analogue state with the beta of its parent have been given in the literature. Most of these have been restricted to cases for which the initial and final state spins differ in order to better insure that the orbital matrix element can be neglected. In Table 3 a summary is given of some of the gamma decay-beta decay comparisons made with analogue states in medium weight ($A > 30$) nuclei. The column headed Γ_β is the quantity

$$\Gamma_\beta = 134.5\ E_\gamma^3/T \cdot ft\ eV$$

which corresponds by virtue of the equation for $\Lambda(M1)/\Lambda(GT)$ and the expressions for $\Gamma_\gamma(M1)$ and the beta decay ft value to the radiative transition width $\Gamma_\gamma(M1)$. The reference cited is the author who has made the comparisons. In some cases the agreement between Γ_γ and Γ_β is fairly good. However, there are a number of cases where the disagreement is significant. One of the possible reasons for the discrepancy in these cases is the experimental difficulty of determining absolute radiative widths. Endt (1967) has discussed this problem. On the other hand, some of the deviations are probably real. A possible explanation for this is that the orbital matrix element contributes significantly to the ratio $\Lambda(M1)/\Lambda(GT)$.

D. Statistics

In Chapter V of this dissertation, special attention is given to correlations between various sets of absolute widths. The quantitative measure that is used to determine such correlations is the linear correlation coefficient (LCC). Basically, this quantity is a measure of how much two sets of numbers are linearly related (assuming, of course, that the sets contain the same number of elements). The definition of the linear correlation coefficient for, say, sets of data $X(x_i)$ and $Y(y_i)$ is

$$r = \sqrt{bb'} \quad \text{(Bevington, 1969)}$$

where b and b' are determined from least square fits of $X = a + bY$ and $Y = a' + b'X$. The sign of r is taken to be the same as that of b (and hence b'). Its range is -1.00 to 1.00 with $r = 0$ meaning that X and Y are not correlated and $|r| = 1.00$ meaning that X and Y are perfectly correlated. Unfortunately r does not by itself adequately describe a correlation between sets of data since, for example, correlations involving sets with only two elements will always give $|r| = 1$. Thus one needs to ascribe statistical significance to the LCC, that is, a "confidence factor". Several different definitions of this term are possible. In this dissertation the following is used:

> The confidence factor for a linear correlation coefficient r between two sets of data is the probability of getting a smaller LCC than r (or, if $r < 0$, a value larger than r) if the sets contained only random numbers.

In order to determine confidence factors, then, it is necessary to choose

the proper distribution from which random data would originate. In most applications one would assume a normal distribution. However for nuclear reaction widths, Porter and Thomas (1956) have shown that the parent distribution is the chi-squared distribution of one degree of freedom (the Porter-Thomas distribution). Furthermore, total widths which are the sum of, say, N partial widths are expected to obey the chi-squared distribution of N degrees of freedom assuming that the average reduced width is the same for each channel. These distributions are briefly discussed in Appendix C.

The method for computing confidence factors is to generate sets of random numbers from the prescribed distribution (the procedure for this is discussed in Appendix C), correlate them, and upon choosing a suitable interval size make a histogram of the number of cases having linear correlation coefficients within a given interval (in the range of -1.00 to 1.00). The confidence factor is then obtained directly as the cumulative sum of the histogram entries.

Over the region of a fragmented analogue state, the enhanced reduced widths do not follow the Porter-Thomas distribution. Robson (1969) has shown that the expected enhancement pattern for elastic widths is a skewed Lorentzian (the low energy tail of which is normally called the "Robson Assymetry"). The statistical distribution of the fragments for other exit channels is not well established experimentally. Presumably, if the widths in any channel are Lorentzian and correlated with the

elastic widths they indicate enhancement of that channel. If they are not enhanced, they are expected to obey the Porter-Thomas distribution. Lane (1969) has given the most comprehensive treatments of fine structure and correlations between decay widths in various channels and has shown that enhancement of two or more decay channels implies correlations between their reduced widths. However, no detailed predictions of analogue enhancement of isospin-allowed decay channels other than the elastic have been made.

Chapter III

EQUIPMENT AND EXPERIMENTAL PROCEDURE

These high resolution proton capture experiments were performed on the TUNL 3 MV Van de Graaff accelerator. A schematic of the laboratory as used in elastic scattering experiments is shown in Fig. 2. The electrostatic analyzer-homegenizer system was developed over a period of years and has been described in detail elsewhere (Parks et al., 1958; Seibel, 1968; Lindstrom, 1970). For these (p,γ) experiments, a new, smaller scattering chamber was designed and placed in the beam line about 2 feet in front of the elastic scattering chamber. For beam current integration, an air-cooled Faraday cup (consisting primarily of a 0.015 inch thick, 6 inch in diameter tantalum disc) was attached to the back of the elastic chamber at a distance of about 4 feet from the target. Figure 3 shows the geometry of the chamber and three detectors used in the present experiments.

Figure 2. Floor plan of the 3 MV Van de Graaff laboratory showing the electrostatic analyzer-homogenizer system.

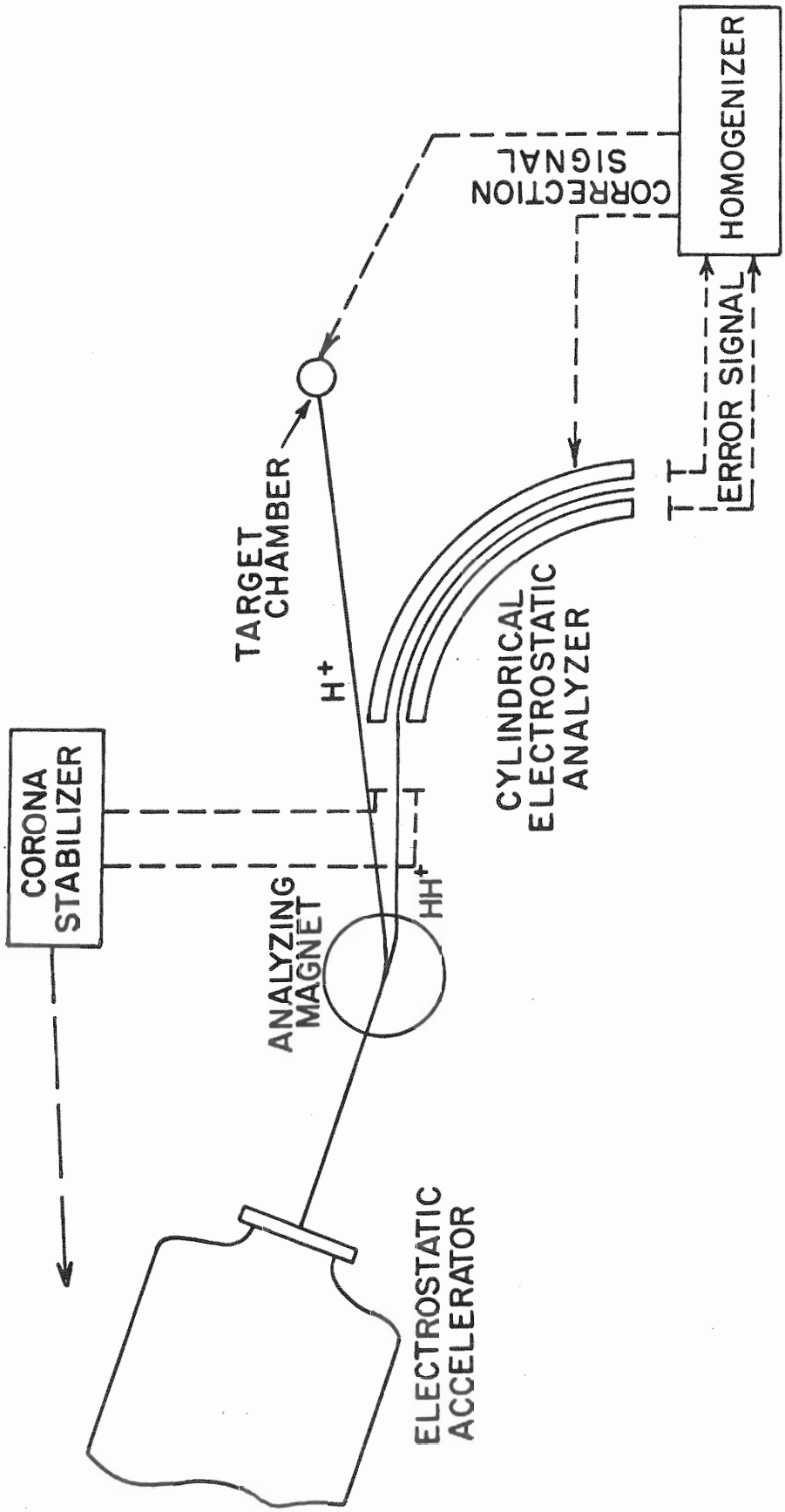
HOMOGENIZER
CORRECTION SIGNAL
ERROR SIGNAL
TARGET CHAMBER
H+
CYLINDRICAL ELECTROSTATIC ANALYZER
CORONA STABILIZER
ANALYZING MAGNET
HH+
ELECTROSTATIC ACCELERATOR

Figure 3. Schematic of the target chamber and detector geometries used in the present experiments. The solid angle for the surface barrier detector was 7.36 millisteradians.

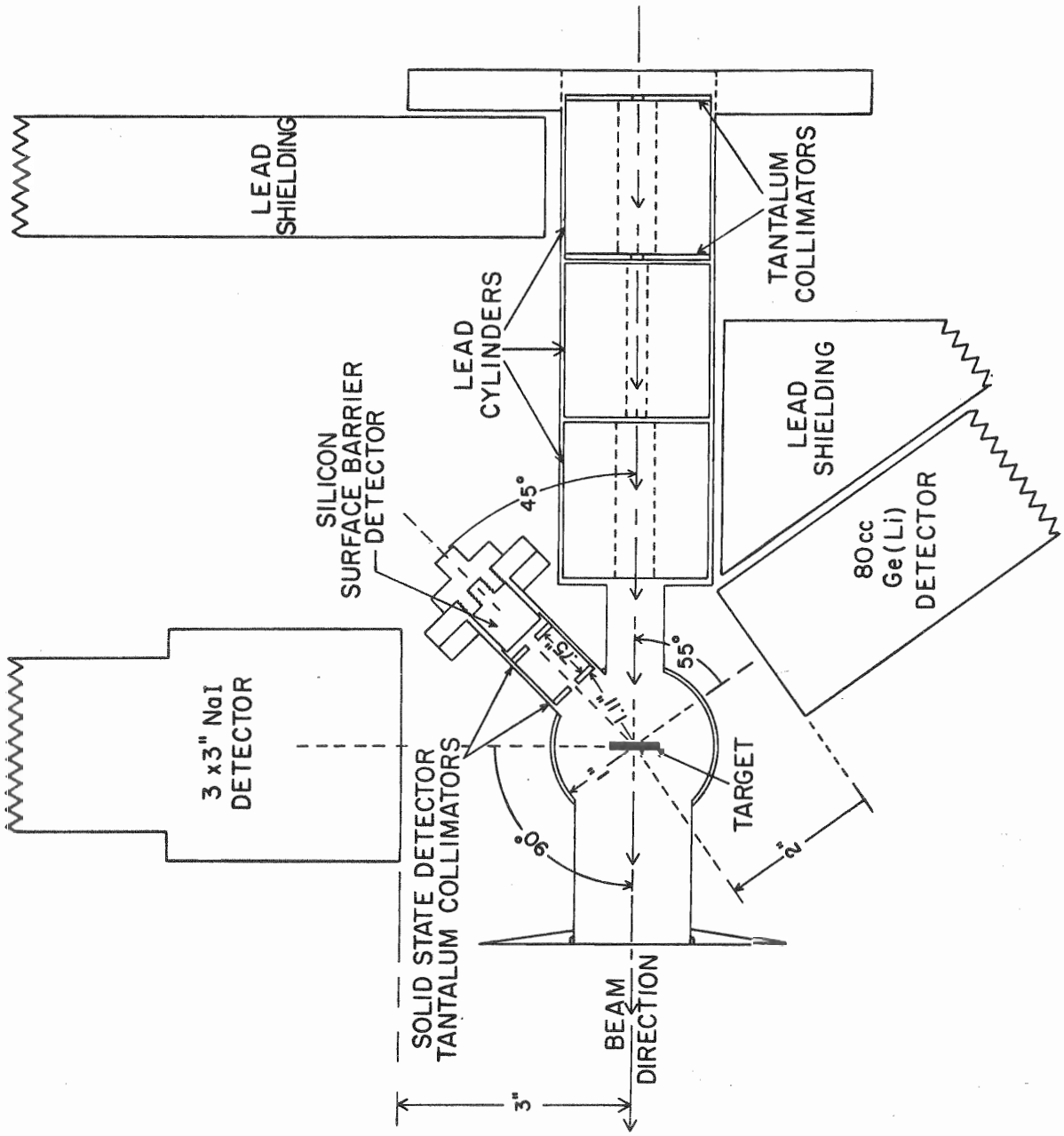
LEAD SHIELDING
TANTALUM COLLIMATORS
LEAD CYLINDERS
SILICON SURFACE BARRIER DETECTOR
45°
LEAD SHIELDING
80cc Ge(Li) DETECTOR
55°
3 x3" NaI DETECTOR
SOLID STATE DETECTOR TANTALUM COLLIMATORS
TARGET
90°
2"
BEAM DIRECTION
3"

A. Detectors

The solid state detector used to observe charged particles was an ORTEC silicon surface barrier detector which had an active area of 50 mm^2, a depletion depth of 300 microns and a resolution (FWHM) of about 12 keV, as determined in these experiments. The bias for this detector was +80 V. The NaI(Tl) detector was a 7.6 cm by 7.6 cm cylindrical crystal (from Harshaw Chemical Company) with a RCA 8575 phototube. A phototube plate voltage of +1250 V (with the detector housing at ground potential) yielded the best resolution, about 10% at 662 keV. The Ge(Li) detector (Princeton Gamma-Tech) had a specified active volume of 80 cm^3 and was operated at -2000 V. The Ge(Li) detector resolution in the present experiments was about 4 keV for the 1332 keV line in ^{60}Co. An absolute efficiency curve for this detector was determined using sources placed in the target position shown in Fig. 3. Details and results of these efficiency measurements are given in Appendix B.

B. Electronics

In the present experiments data were taken with a digital readout system (Lindstrom, 1970) and a Honeywell DDP-224 computer. The digital readout system was used to read data from scalers onto punched cards by means of an IBM keypunch. Figure 4, a block diagram of the

Figure 4. Block diagram of the elastic scattering counting system.

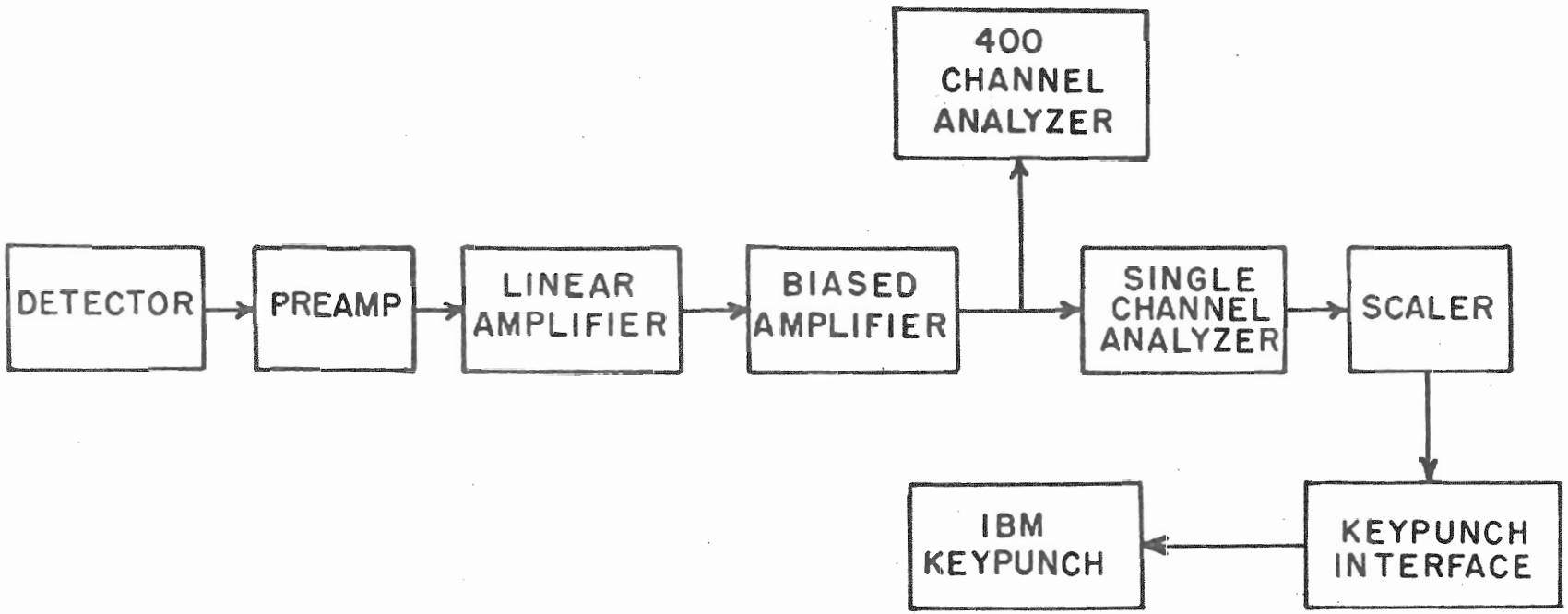
400
CHANNEL
ANALYZER
DETECTOR
PREAMP
LINEAR
AMPLIFIER
BIASED
AMPLIFIER
SINGLE
CHANNEL
ANALYZER
SCALER
IBM
KEYPUNCH
KEYPUNCH
INTERFACE

electronics used with the solid state (elastic) detector, illustrates the use of this device. The method for accumulating elastic scattering data has been described by Moses (1970), Lindstrom (1970), and Prochnow (1971) and will not be discussed here. The primary use of the DPP-224 computer was as a multichannel analyzer (4096 channels for Ge(Li) spectra and 512 channels for NaI(Tl) spectra). In Fig. 5 a block diagram is given of the electronics used with the two gamma ray detectors. When measuring NaI(Tl) yield curves, the output of the amplifier was connected to the computer through an analog to digital converter (ADC). Otherwise, the output went to a single channel analyzer (SCA) whose discriminators were set for a specified gamma ray energy range, usually 1 to 5 MeV. The SCA output was counted by a scaler and monitored with a ratemeter.

As shown in Fig. 5, the electronics for the Ge(Li) detector was quite similar to that for the NaI(Tl) detector. However, when measuring Ge(Li) spectra some additional electronics were required in order to measure the fraction of time that the ADC was busy analyzing input pulses and not available to process incoming data (the fraction of time that the ADC is busy is usually called the dead time). A block diagram of the electronics used in the dead time measurements is shown in Fig. 6. The isolation module separated the computer and 3 MeV Laboratory electrical grounds and is discussed in Appendix D. The scaler control circuit was designed to provide the correct voltages for the various gate signals

Figure 5. Block diagram of the electronics for the Ge(Li) and NaI(Tl) detectors.

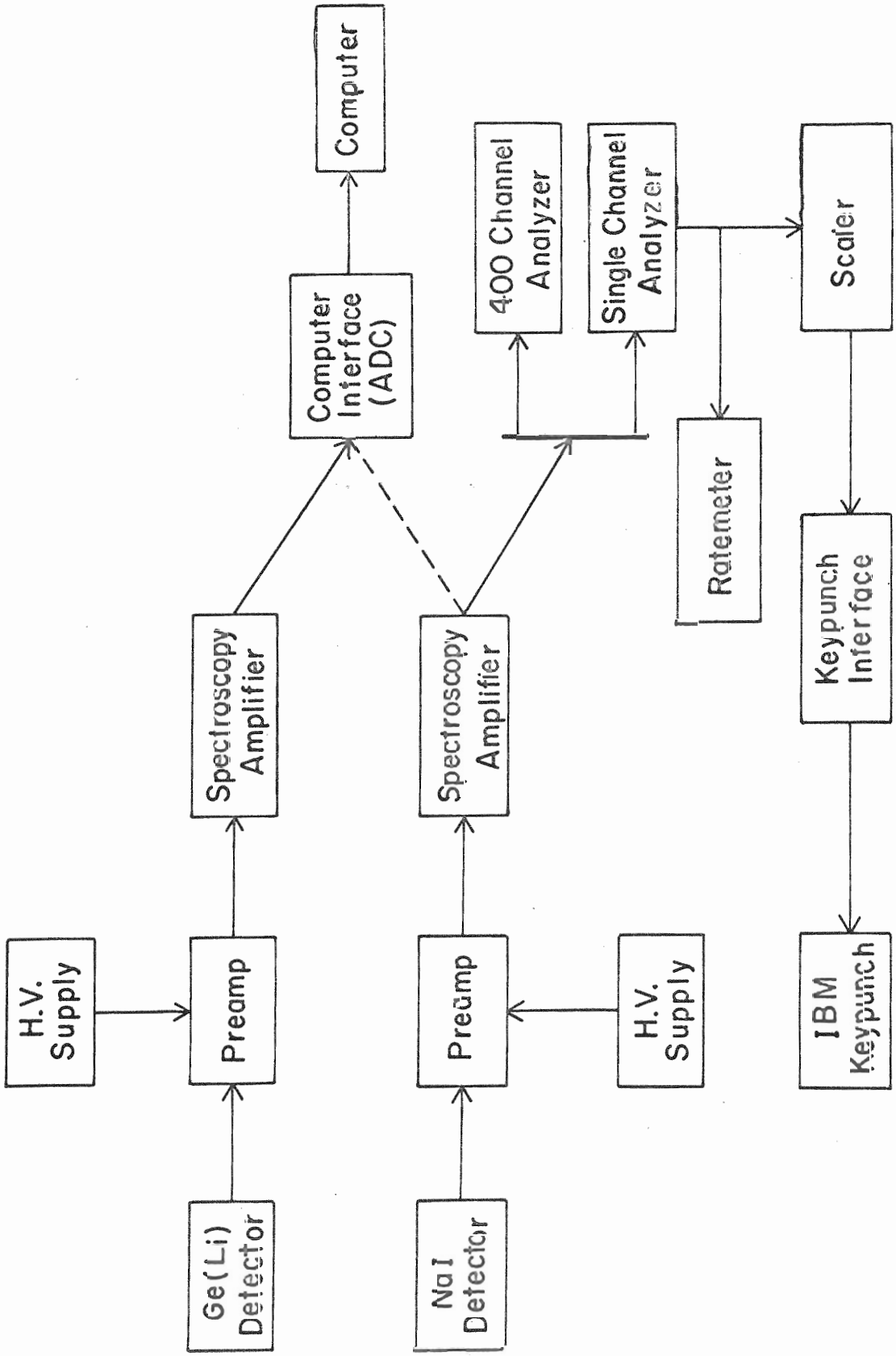
Computer
Computer Interface (ADC)
400 Channel Analyzer
Single Channel Analyzer
Scaler
Ratemeter
Keypunch Interface
IBM Keypunch
Spectroscopy Amplifier
Spectroscopy Amplifier
H.V. Supply
Preamp
Preamp
H.V. Supply
Ge(Li) Detector
NaI Detector

Figure 6. Block diagram of the dead time monitoring system.

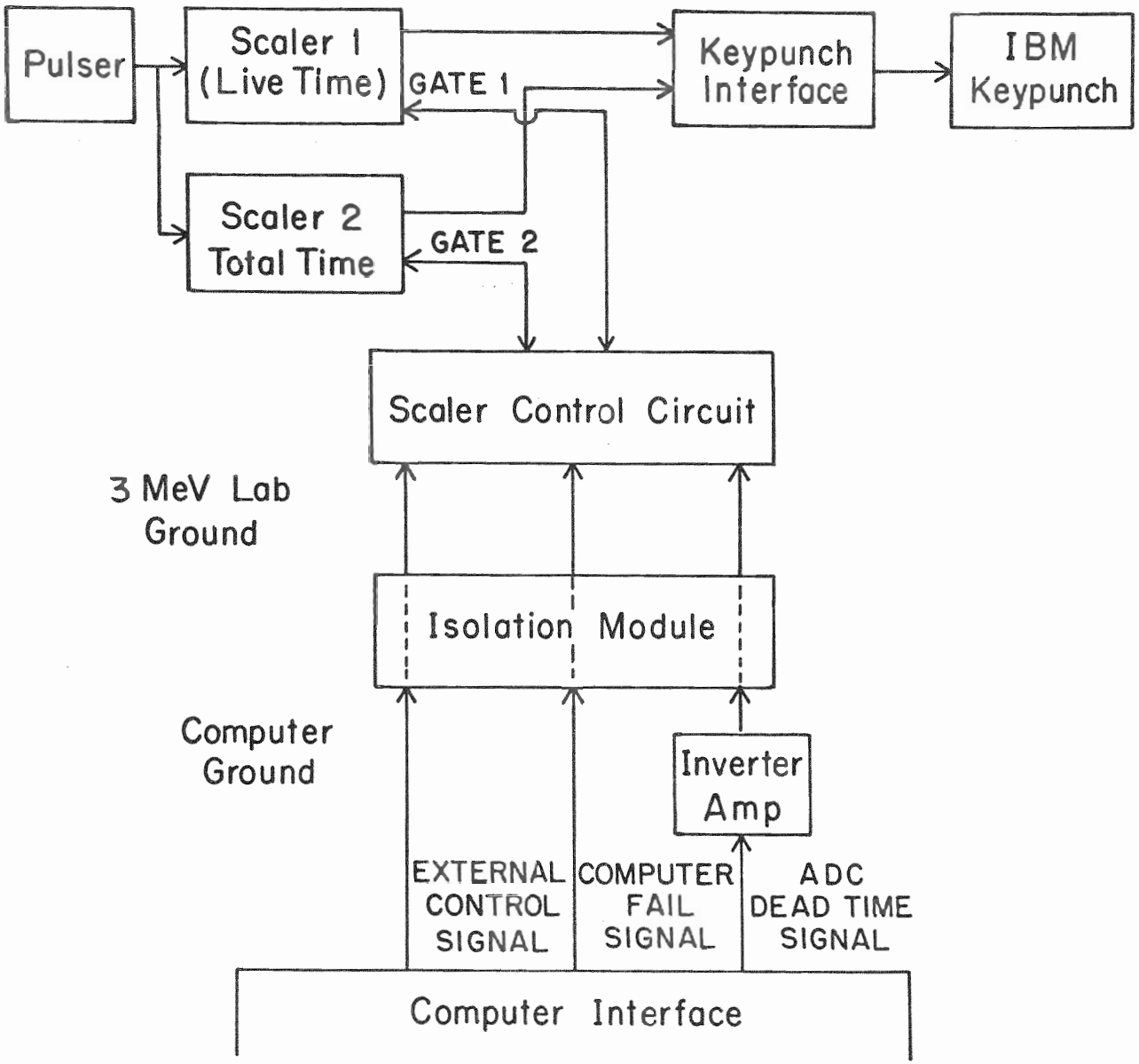
Pulser
Scaler 1
(Live Time)
GATE 1
Keypunch
Interface
IBM
Keypunch
Scaler 2
Total Time
GATE 2
Scaler Control Circuit
3 MeV Lab
Ground
Isolation Module
Computer
Ground
Inverter
Amp
EXTERNAL
CONTROL
SIGNAL
COMPUTER
FAIL
SIGNAL
ADC
DEAD TIME
SIGNAL
Computer Interface

shown in the drawing. Gate 1 was the ADC busy signal and Gate 2 (which was also applied to Scaler 1 by way of the keypunch interface) was an external control signal sent by the computer when the ADC was off. The computer fail signal also gated both scalers. Typical values of the dead time were on the order of 2%.

C. Target Preparation

Targets were prepared by evaporation of enriched metallic Cr powder and Fe_2O_3 onto 10 $\mu g/cm^2$ carbon foils. The specific enrichments of the isotopes are listed in Table 4.

The evaporations were performed with vacuums of between 10^{-5} and 10^{-6} torr. For the ^{54}Cr isotope, a 0.010 inch thick tungsten boat heated to about 1275° C was used. A typical elastic scattering spectrum of targets made by this method is shown in Fig. 7. Because the temperature required for the Fe evaporations is about 1600° C (in a vacuum of 10^{-6} torr), it was decided not to evaporate these isotopes from a tungsten boat because tungsten oxide evaporates at about 1300° C. Previous experiments by Lindstrom (1970) used targets evaporated from tungsten boats and the targets had fairly large tungsten impurities. The method finally adopted was to evaporate the Fe isotopes from a deep (1 inch) carbon crucible. Each oxide was heated in a crucible until reduction took place (no catalysts were necessary). This reduction occurred

Table 4. Target Composition

Isotope	% Enrichment	Contaminant	%
^{54}Cr (Metal Powder)	94.35	^{50}Cr	0.08
		^{52}Cr	3.26
		^{53}Cr	2.31
^{54}Fe (Oxide)	98.19	^{56}Fe	1.81
		^{57}Fe	0.05
		^{58}Fe	0.05
^{56}Fe (Oxide)	99.93	^{54}Fe	0.03
		^{57}Fe	0.03
		^{58}Fe	0.02
^{58}Fe (Oxide)	82.48	^{54}Fe	0.46
		^{56}Fe	15.57
		^{57}Fe	1.48

Figure 7. Typical charged particle spectrum for the ^{54}Cr isotope.

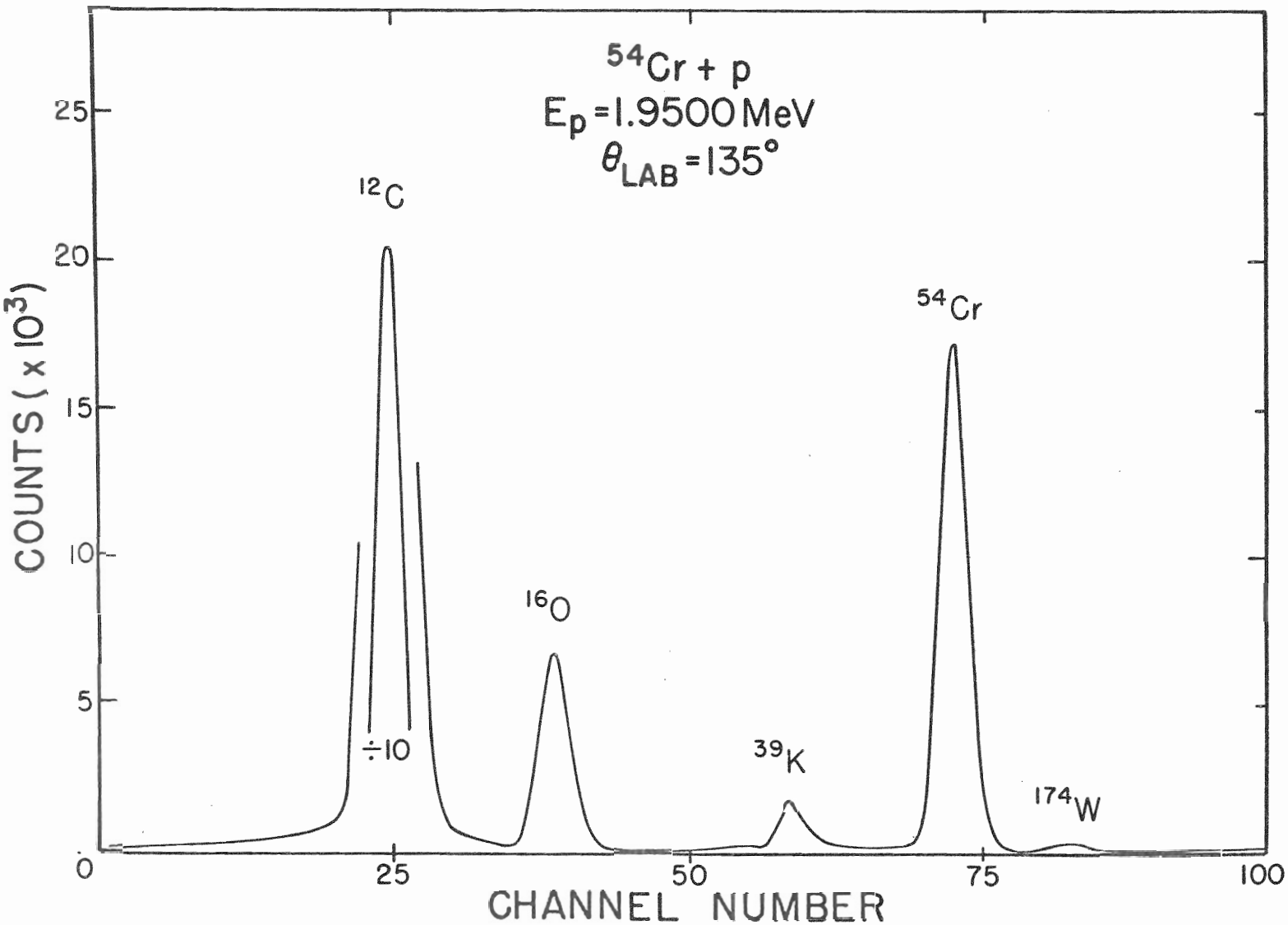
^{54}Cr + p
E_p = 1.9500 MeV
θ_{LAB} = 135°
^{12}C
^{16}O
^{39}K
^{54}Cr
^{174}W
÷10
COUNTS (x 10^3)
CHANNEL NUMBER
0
5
10
15
20
25
25
50
75
100

at 1100 to 1200° C, depending upon the vacuum. During reduction some care was required to insure that the Fe_2O_3 did not spatter out of the crucible. Figure 8 shows a typical ^{58}Fe elastic scattering spectrum for targets made from this method. High mass contaminants present in Fe targets evaporated from tungsten boats have been effectively eliminated. Typical target thicknesses obtained from these methods were between 1 and 3 $\mu g/cm^2$.

The total energy resolution obtained in these experiments with targets prepared by the above methods was between 300 and 450 eV, depending upon the target thickness. This resolution - hereafter in this dissertation referred to as the proton energy resolution - includes the contributions from the energy spread of the incident proton beam, target Doppler broadening, and target thickness.

Concern has been expressed (Endt, 1967) that the measurement of absolute gamma decay widths may depend on the atomic form of the isotope when evaporated. Leslie et al. (1971A) have shown that, within the limits of experimental error, the absolute widths obtained from targets prepared by evaporation of Fe metal and Fe_2O_3 are in agreement.

D. Reduction of Data

For thin targets the relationship between the yield of gamma

Figure 8. Typical charged particle spectrum for the ^{58}Fe isotope.

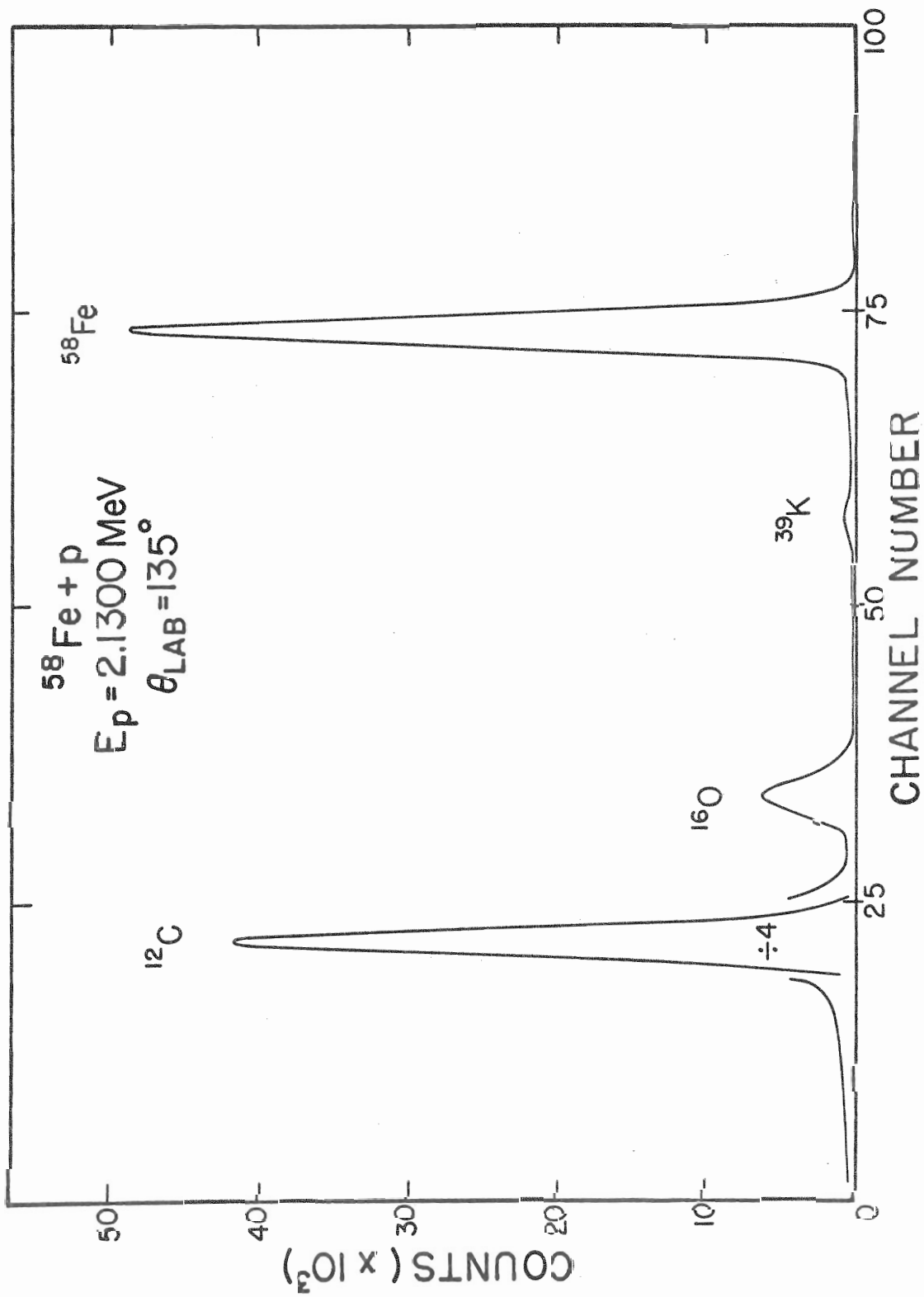
^{58}Fe + p
E_p = 2.1300 MeV
θ_{LAB} = 135°
^{12}C
÷4
^{16}O
^{39}K
^{58}Fe
COUNTS (x 10^3)
CHANNEL NUMBER
0
10
20
30
40
50
25
50
75
100

rays from a proton induced resonance and the corresponding partial gamma decay width is

$$\frac{2J+1}{2J_o+1} \quad \frac{\Gamma_p \Gamma_\gamma}{\Gamma} = \frac{4\epsilon}{\lambda^2} \left(\frac{Y}{T} \right) \quad \text{(Gove, 1959)},$$

where

J = spin of the compound nuclear state

J_o = spin of the target

Γ_p = proton elastic width

Γ_γ = partial gamma decay width

Γ = total width

ϵ = stopping power of the target in eV cm^2

λ = center of mass wavelength of the incident protons in cm

T = target thickness in eV

and Y = area of the (Breit-Wigner) resonances in units of reactions times energy per incident particle.

The equation for thick targets (targets whose thickness in units of energy is many times greater than the total width Γ) is the same as the above except that $Y/T = Y'$ is in this case the step in the gamma ray yield in units of reactions per incident particle.

The thin target yield for proton induced resonances on spin zero targets can be written as

$$(2J+1)\, \Gamma_p \Gamma_\gamma / \Gamma = 4Y/B\lambda^2 t ,$$

where t = target thickness in $\mu g/cm^2$, by virtue of the relation for the

stopping power

$$\epsilon = \frac{1}{B}\frac{dE}{dx} \quad .$$

This last equation for $\Gamma_p \Gamma_\gamma / \Gamma$ was used to obtain the absolute widths for transitions to low-lying levels from resonances in the regions of the ground state analogues in ^{55}Mn and ^{59}Co. The parameters in this equation were determined in the following manner:

1. J, the resonance spin, was determined from results of elastic proton scattering given by Moses (1970) for ^{55}Mn and Lindstrom (1970) for ^{59}Co. The elastic cross sections over both of these analogue state regions were remeasured as part of these experiments in order to verify the spin assignments and elastic widths. The method used to analyze these data has been described in detail by Prochnow (1971) and will not be discussed here. Several levels in the region of the ^{59}Co ground state analogue were found to have been assigned incorrect spins (the up-dated assignments are given in Chapter IV).

2. Γ_p was also obtained from the elastic scattering experiments. Since $\Gamma = \Gamma_p + \Gamma_{\gamma\ \text{total}} + \Gamma_{p'}$ (no other channels are open) and since $\Gamma_{\gamma\ \text{total}}$ and $\Gamma_{p'}$ were observed to be much smaller than Γ_p, the approximation $\Gamma_p / \Gamma = 1$ was made.

3. The B parameters in the stopping power equation were taken from a tabulation by Marion (1960). When required, the dE/dx energy losses were calculated with the computer code BABEL (written by P. G. Ikossi). This code is based on the method of Barkas and Berger (1964). Comparisons of calculated values obtained from BABEL for ^{58}Ni and ^{27}Al with data given by Marion (1968) showed agreement to within a few percent.

4. $$\lambda^2 = \left[\frac{A+1}{A}\right]^2 \frac{h^2}{2ME_p}$$

where A = N + Z of the target

h = Planck's constant

M = atomic mass of the target

and E_p = laboratory energy of the incident protons.

5. The target thickness, t, was determined from Rutherford scattering immediately prior to the gamma ray yield measurements.

6. $Y = N\ R\ Area/(Eff(E_\gamma) \cdot I_c)$

where a) N was a normalization factor which included the dead time correction and a correction for target deterioration. Explicitly (Live Time = Total Time - Dead Time)

$$N = \frac{\text{Count Ratio}}{\text{Live Time/Total Time}} \cdot$$

$$\text{The Count Ratio} = \frac{Ci}{C_{total}} \times \frac{BCI}{Qi} ,$$

where Ci was the number of counts measured by the NaI(Tl) detector for a given amount of integrated charge Qi (usually 1000 μC) at the beginning of a Ge(Li) spectrum and C_{total} was the number of counts measured by the NaI(Tl) detector for the total beam current integration, BCI. In the present experiments, the BCI was usually 50,000 μC, which required about 2 1/2 hours per Ge(Li) spectrum for a typical beam of 5 μ amps. Typical values of N were between 1.05 and 1.10.

b) R was the ratio of area to peak height for the resonance. This parameter was obtained from area analysis of a 2 to 5 keV NaI(Tl) yield curve taken just before the Ge(Li) spectrum. This correction was required because the Ge(Li) spectra were taken at the resonant energies rather than taking spectra at 100 eV intervals over each resonance. The time required to take Ge(Li) spectra over an entire resonance, 20 hours or more, was prohibitive in view of the large number of resonances (32) to be

studied. Since the proton energy resolution in these experiments (300 to 500 eV) was much greater than the total width for any of the resonances that were studied, all of the observed widths were equal to the resolution. The peak height for each of these resonances was therefore quite sensitive to the proton energy resolution. (On the other hand, the total area of a resonance does not depend on the resolution.) Unfortunately, the proton energy resolution did not remain constant during the time required for several Ge(Li) spectra because of target deterioration. Typically, R ranged from 3.5 for a new target (for which the resolution was 300 eV) to 5.5 for the same target after 18 hours of 5.0 μamp of beam (for which the resolution was 500 eV).

c) Area = area of the photopeak in the Ge(Li) spectrum. This parameter was obtained by standard area analysis techniques (for example, Bevington, 1969). Identification of the transitions (in the compound nuclei ^{55}Mn and ^{59}Co) which were associated with the peaks in the Ge(Li) spectra was made entirely from energy considerations. The energies

were determined from a channel-energy calibration curve which was a least square fit of calibration points from a ^{56}Co source (Marion, 1968) and the well-known 992 keV resonance in $^{27}Al(p,\gamma)^{28}Si$ (Holmberg and Kiuru, 1970).

d) $Eff(E_\gamma)$ was the absolute efficiency of the Ge(Li) detector at the photopeak energy. The efficiency measurements are discussed in Appendix B.

e) I_c was the number of incident protons, namely,

$$I_c = \frac{BCI}{1.6 \times 10^{-19} \text{ C/Proton}} .$$

For the resonances in ^{55}Mn and ^{59}Co, the energies of the gamma rays associated with the inelastic decays were high enough (835 keV and 810 keV, respectively) so that the inelastic widths, $\Gamma_{p'}$, could be determined from the equation for the gamma ray yield. The absolute width equation can be written

No. of Counts = No. of Incident Protons X Stopping Factors X Probability for Formation of Resonance X Probability for Decay.

The probability for decay into channel c is $\Gamma c/\Gamma$. All other terms, except the number of counts, refer to the incident channel. Since the number of inelastic protons is equal to the number of "inelastic" gamma rays, the absolute widths obtained from the 810 and 835 keV gamma rays were the inelastic widths, $\Gamma_{p'}$.

Chapter IV

EXPERIMENTAL RESULTS

Because of the importance of the resonance spins and elastic widths, the elastic cross sections over the analogue state regions in ^{55}Mn and ^{59}Co were remeasured. The agreement with the previous ^{55}Mn results (Moses, 1970) was excellent. These data are presented in Table 5. The energies given in this table have been assigned from a recalibration of the Van de Graaff accelerator (using the ^{7}Li(p,n) threshold). Specifically, the laboratory energy of the largest $3/2^-$ state in the analogue region (Γ_p = 115 eV) was measured to be 1.9875 MeV with an estimated uncertainty of 1 keV. The inelastic widths, $\Gamma_{p'}$, were determined in the present experiments. The estimated minimum level of observability of the inelastic widths determined from the yield of gamma rays (associated with the inelastic decay) is 0.005 eV, much smaller than that from charged particle detection. In the charged particle elastic scattering experiments on the IAS in ^{55}Mn and ^{59}Co, no inelastic protons were observed because of the charged particle background and short counting times ($\sim$ 30 sec).

Table 5. ^{55}Mn Resonance Parameters in the Vicinity of the Ground State Analogue.

E_p (MeV)	J^π	Γ_p (eV)	γ_p^2 (keV)	$\Gamma_{p'}$ (eV)
1.9586	$(1/2^+)$	5 ± 3	0.22	0.011
1.9635	$(3/2)^-$	10 ± 5	0.11	0.140
1.9777	$1/2^+$	13 ± 5	0.55	0.026
1.9788	$1/2^+$	9 ± 5	0.38	0.029
1.9842	$(3/2)^-$	10 ± 5	1.00	0.092
1.9875	$3/2^-$	115 ± 10	10.97	0.501
1.9929	$(3/2)^-$	20 ± 5	1.87	0.218
2.0020	$3/2^-$	40 ± 5	3.61	0.278
2.0059	$(3/2)^-$	20 ± 5	1.78	0.297
2.0075	$(3/2)^-$	25 ± 5	2.21	0.192
2.0089	$3/2^-$	55 ± 5	4.83	0.545
2.0113	$3/2^-$	65 ± 7	5.65	0.349

For the ground state analogue in ^{59}Co, the agreement with the previous elastic scattering results (Lindstrom, 1970) was not as good. Part of the discrepancy can be attributed to the level density in ^{59}Co and the total energy resolution obtained in the two experiments. The energy resolution for Lindstrom's experiments was about 350 to 450 eV and several doublets were therefore not resolved. The proton energy resolution for the present elastic scattering experiments was between 300 and 350 eV. Another possible explanation for the misassignments made in the earlier work is that the large tungsten contaminant present in those experiments could have appreciably affected the 90 degree data (which was crucial to the identification of s-waves). The revised parameters from the present work are listed in Table 6. It should be emphasized that due to the disagreement with the earlier work much of the data was retaken several times in order to confirm the present assignments. The energies of the resonances given in Table 6 were determined by overlapping the $^{58}Fe(p,\gamma)$ and $^{54}Cr(p,\gamma)$ NaI(Tl) yield curves. The energy of the strongest $3/2^-$ state (Γ_p = 100 eV) was measured in this manner to be 2.2237 MeV with an uncertainty of about 3 keV.

A. $^{54}Cr(p,\gamma)^{55}Mn$

The spin and parity of the ground state analogue in ^{55}Mn is $3/2^-$. As shown in Table 5, there are eight resolvable fine structure

Table 6. ^{59}Co Resonance Parameters in the Vicinity of the Ground State Analogue.

E_p (MeV)	J^π	Γ_p (eV)	γ_p^2 (keV)	$\Gamma_{p'}$ (eV)
2.1389	$1/2^+$	10 ± 5	0.45	0.042
2.1513	$1/2^+$	7 ± 3	0.30	0.041
2.1650	$1/2^+$	20 ± 5	0.82	0.074
2.1745	$1/2^+$	10 ± 5	0.40	0.081
2.1888	$1/2^+$	16 ± 5	0.60	0.430
2.1896	$1/2^+$	21 ± 5	0.79	0.214
2.1996	$(1/2^+)$	≤ 5	0.19	0.220
2.2020	$1/2^+$	12 ± 5	0.43	0.339
2.2133	$(3/2)^-$	20 ± 5	1.65	0.463
2.2167	$(3/2)^-$	14 ± 5	1.09	0.538
2.2172	$1/2^+$	27 ± 7	0.93	0.504
2.2203	$(3/2)^-$	10 ± 5	0.76	0.038
2.2226	$(3/2)^-$	10 ± 5	0.76	0.279
2.2237	$3/2^-$	100 ± 20	7.60	1.406
2.2278	$1/2^+$	25 ± 12	0.83	1.366
2.2280	$3/2^-$	55 ± 25	4.12	
2.2297	$(3/2)^-$	10 ± 5	0.74	0.610
2.2340	$(3/2)^-$	15 ± 5	1.10	0.269
2.2360	$1/2^+$	12 ± 5	0.39	0.201
2.2730	$1/2^+$	20 ± 5	0.57	1.291
2.2746	$(3/2)^-$	10 ± 5	0.64	0.097
2.2818	$1/2^+$	25 ± 5	0.70	0.112
2.2983	$(3/2)^-$	12 ± 5	0.71	0.069

components seen in elastic scattering which are in the energy range 1.98 to 2.02 MeV. Since the proton separation energy in ^{55}Mn is 8.0652 MeV (Auble and Rapaport, 1970), the excitation energy of these resonances in the compound nucleus is about 10.0 MeV. The low-lying levels in ^{55}Mn are fairly well known up to about 3.2 MeV. A level scheme for levels below 3.04 MeV (from Auble and Rapaport, 1970) is shown in Fig. 9. Excitation curves taken over the analogue state region (with the NaI(Tl) detector) reveal approximately 3 times as many resonances as observed in elastic scattering. In Fig. 10 this excitation curve is shown along with the elastic data of Moses (1970). The line through the elastic data represents a fit to the data using a multilevel, multichannel R-Matrix code (a discussion of this code is given by Prochnow, 1971). The lines through the gamma ray yield curves have only been included to aid in identifying resonances. The excitation curve with $E_\gamma < 8.5$ MeV includes essentially only the ground state and first excited state transitions (the transitions to the first excited state were found to be quite weak in the case of the p-wave resonances). The excitation curve with $1.5 > E_\gamma > 3.0$ MeV includes the secondary transitions to the ground state from the (at least potential) antianalogue states at 1.528-, 2.251-, 2.564- and 3.045 MeV.

Ge(Li) spectra have been taken on each of the 8 fragments seen in the elastic scattering experiments. A typical spectrum is shown in Fig. 11. The gamma rays associated with the transitions to the ground

Figure 9. Level scheme for ^{55}Mn. The heavier lines indicate the levels to which transitions from the fragments were most often observed.

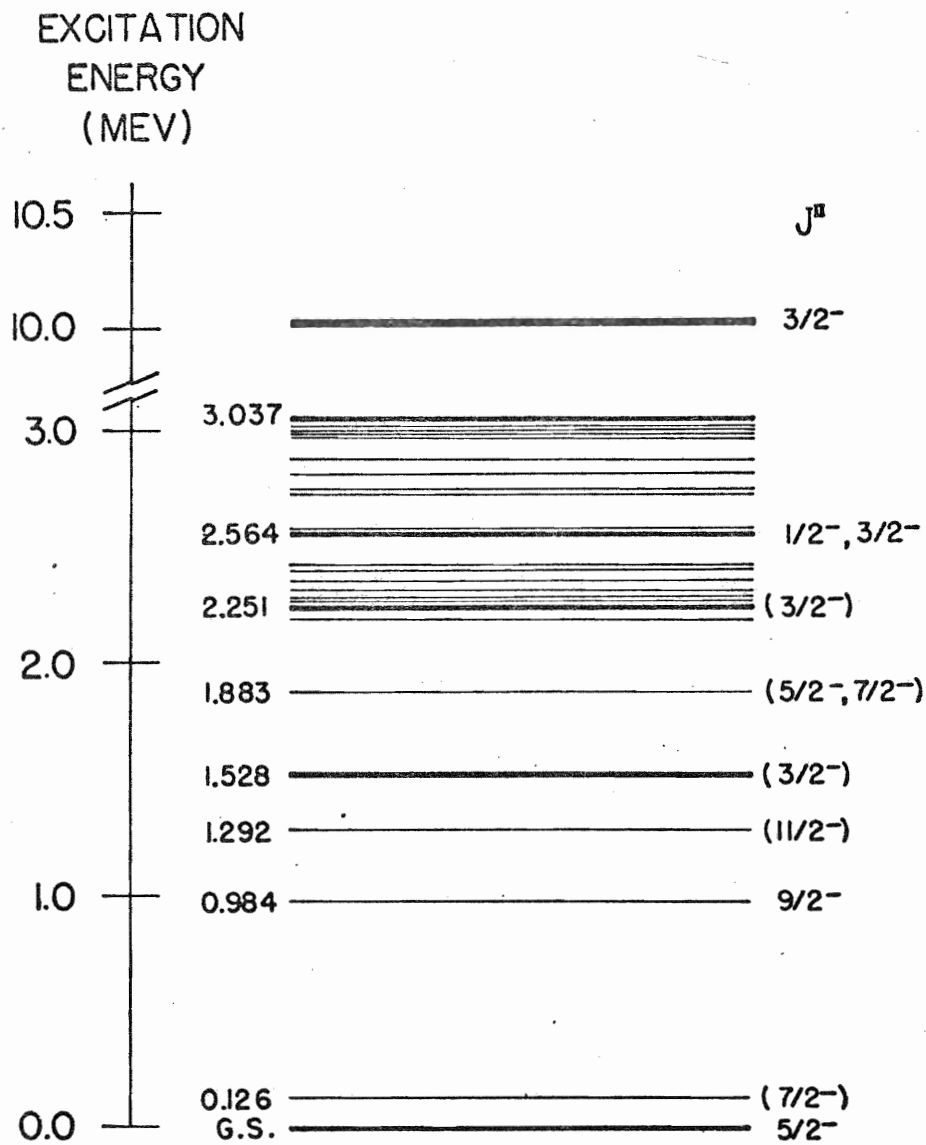
EXCITATION
ENERGY
(MEV)
10.5
10.0
3.0
2.0
1.0
0.0
Jπ
3.037
3/2⁻
2.564
1/2⁻, 3/2⁻
2.251
(3/2⁻)
1.883
(5/2⁻, 7/2⁻)
1.528
(3/2⁻)
1.292
(11/2⁻)
0.984
9/2⁻
0.126
(7/2⁻)
G.S.
5/2⁻

$^{55}_{25}M_{N_{30}}$

Figure 10. Elastic scattering and NaI(Tl) excitation curves over the ground state analogue in ^{55}Mn.

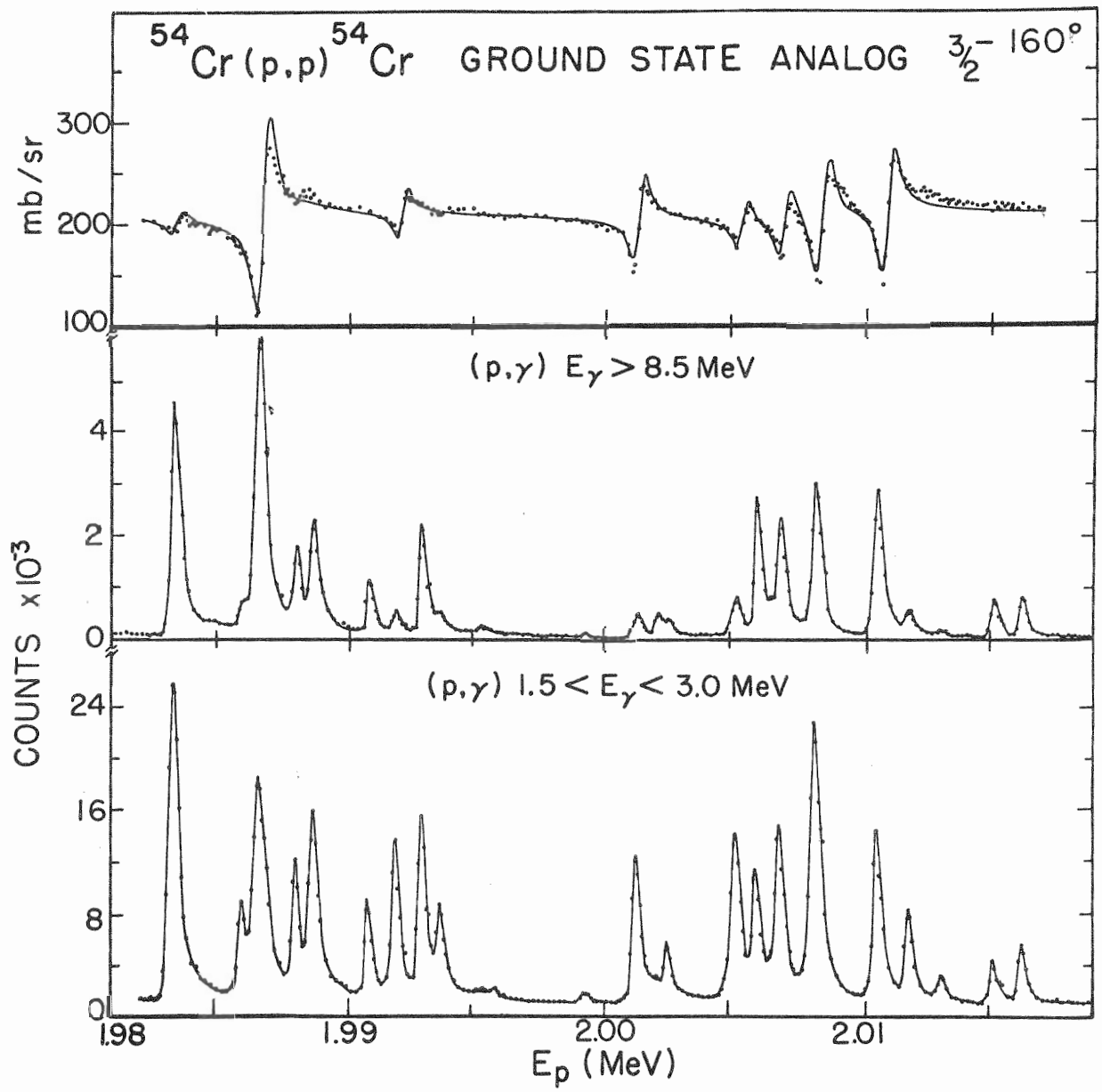
$^{54}Cr(p,p)^{54}Cr$ GROUND STATE ANALOG $3/2^-$ 160°
mb/sr
300
200
100
(p,γ) $E_\gamma > 8.5$ MeV
4
2
0
COUNTS x 10^3
(p,γ) $1.5 < E_\gamma < 3.0$ MeV
24
16
8
0
1.98
1.99
2.00
2.01
E_p (MeV)

Figure 11. A typical $^{54}Cr(p,\gamma)^{55}Mn$ Ge(Li) spectrum.

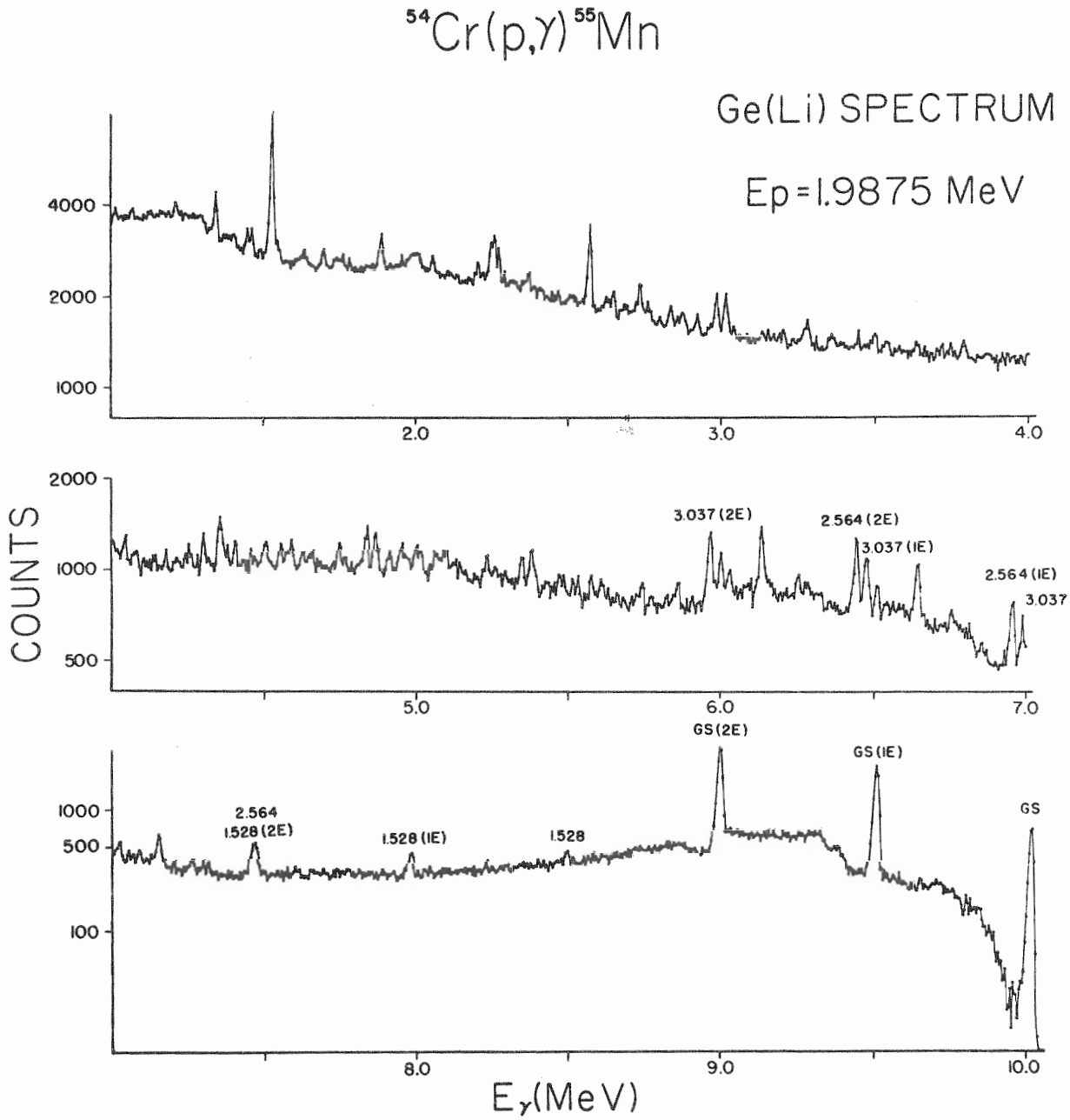
$^{54}Cr(p,\gamma)^{55}Mn$
Ge(Li) SPECTRUM
Ep=1.9875 MeV
COUNTS
4000
2000
1000
2.0
3.0
4.0
2000
1000
500
3.037 (2E)
2.564 (2E)
3.037 (1E)
2.564 (1E)
3.037
5.0
6.0
7.0
GS (2E)
GS (1E)
GS
1000
500
100
2.564
1.528 (2E)
1.528 (1E)
1.528
8.0
9.0
10.0
E_γ(MeV)

state and to the levels at 1.528-, 2.564- and 3.037 MeV have been labelled. In Fig. 12, the absolute widths obtained from the Ge(Li) spectra are plotted. These widths and also the absolute widths for the two s-wave resonances at 1.9777 and 1.9788 MeV are tabulated in Appendix A. A lower limit on the total gamma decay width for each fragment can be estimated from the sum of the partial gamma decay widths for the primary transitions that were observed in the present experiments. A second estimate of the total gamma decay width has been obtained from the absolute widths corresponding to the stronger secondary transitions from well-identified low-lying levels to the ground state. Both of these estimates have been included in Appendix A.

B. $^{58}Fe(p,\gamma)^{59}Co$

The spin and parity of the ground state analogue in ^{59}Co is also $3/2^-$. As listed in Table 6, there are ten fragments resolved in the elastic scattering experiments in the energy range 2.20 to 2.30 MeV. Since the proton separation energy in ^{59}Co is 7.370 MeV (Vervier, 1968), the excitation energy of the ground state analogue is about 9.5 MeV. The low-lying levels in ^{59}Co are not as well identified as those in ^{55}Mn. Figure 13 shows the most recent level scheme (Vervier, 1968) with the known $3/2^-$ states and the ground state labelled. The NaI(Tl) excitation curve taken over a broad region around the analogue state indicates about

Figure 12. Absolute gamma decay widths for the 8 fragments of the ground state analogue in ^{55}Mn. E_{ex} (MeV) is the energy of the final state in the transition from the resonance.

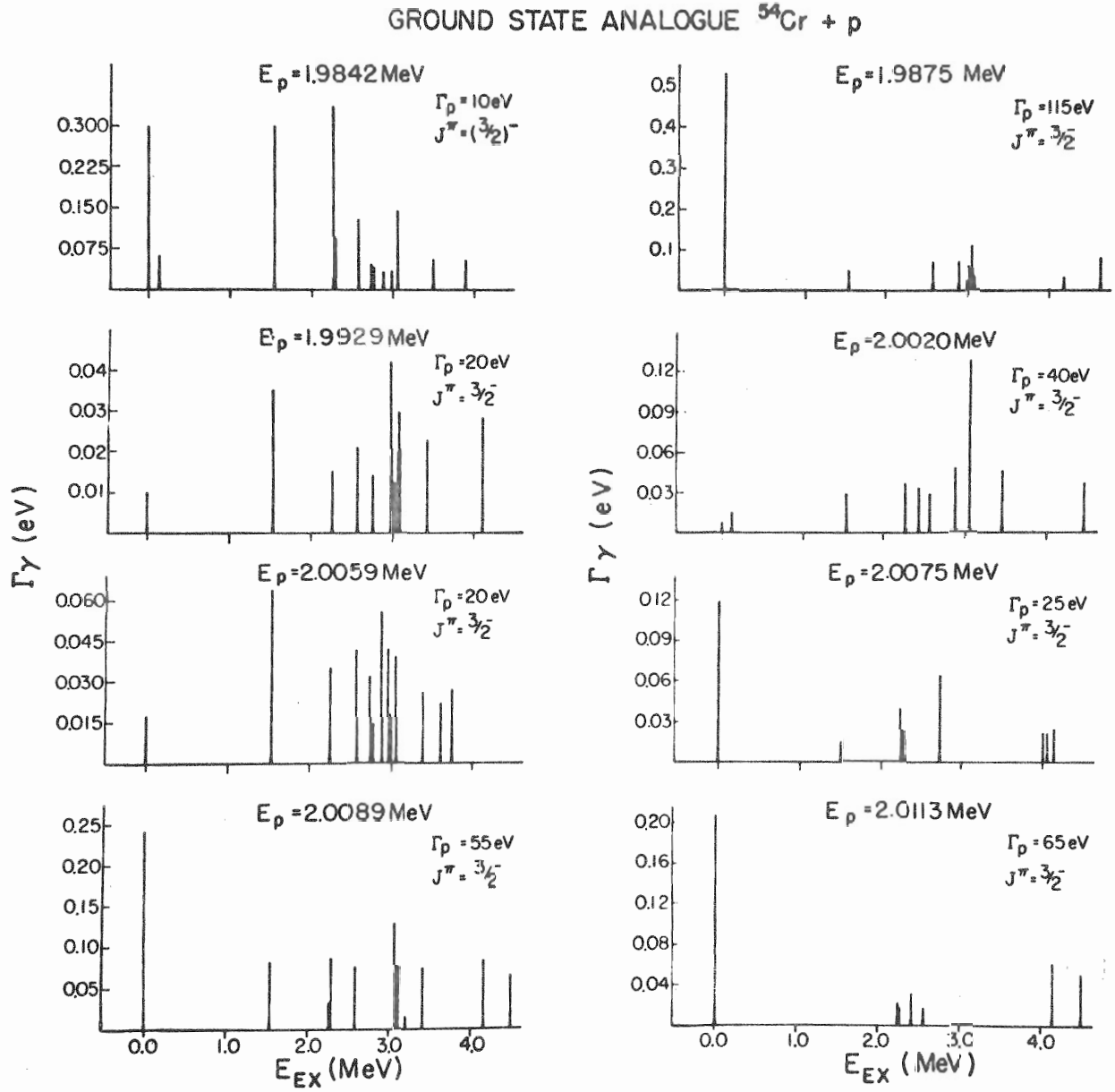
GROUND STATE ANALOGUE $^{54}Cr + p$
E_p = 1.9842 MeV
Γ_p = 10eV
$J^\pi = (3/2)^-$
E_p = 1.9875 MeV
Γ_p = 115eV
$J^\pi = 3/2^-$
E_p = 1.9929 MeV
Γ_p = 20eV
$J^\pi = 3/2^-$
E_p = 2.0020 MeV
Γ_p = 40eV
$J^\pi = 3/2^-$
E_p = 2.0059 MeV
Γ_p = 20eV
$J^\pi = 3/2^-$
E_p = 2.0075 MeV
Γ_p = 25eV
$J^\pi = 3/2^-$
E_p = 2.0089 MeV
Γ_p = 55eV
$J^\pi = 3/2^-$
E_p = 2.0113 MeV
Γ_p = 65eV
$J^\pi = 3/2^-$
$\Gamma\gamma$ (eV)
E_{EX} (MeV)

Figure 13. Level scheme for ^{59}Co. The heavier lines indicate levels to which transitions from the fragments were most often observed.

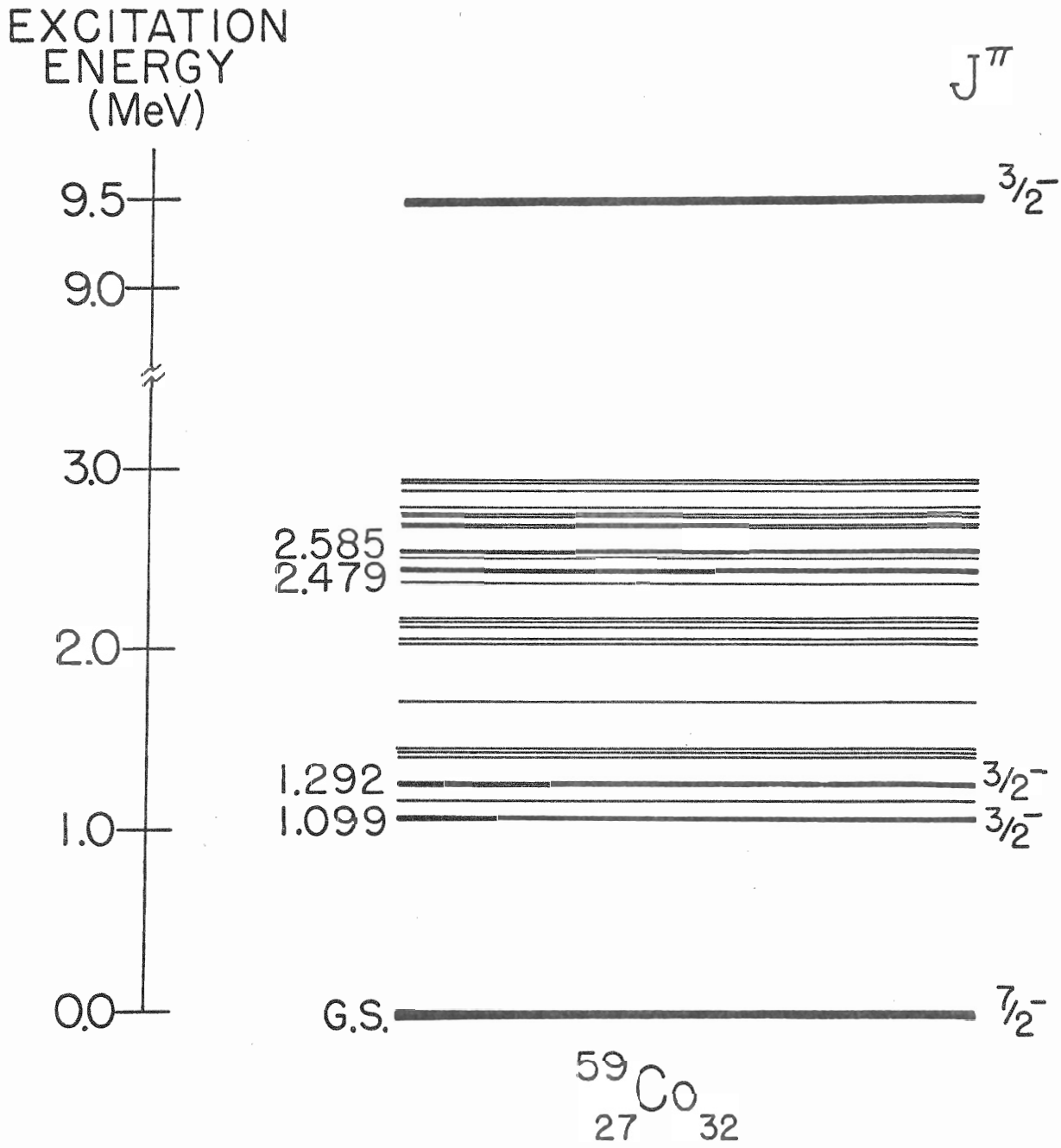
EXCITATION ENERGY (MeV)
J^π
9.5
9.0
3.0
2.0
1.0
0.0
$3/2^-$
2.585
2.479
1.292
1.099
$3/2^-$
$3/2^-$
G.S.
$7/2^-$
$^{59}_{27}Co_{32}$

6 times as many levels as observed in the elastic scattering. This excitation curve is shown in Fig. 14 with the elastic scattering cross section. In this figure, $\ell = 0$ and $\ell = 1$ resonances - as determined from the present elastic scattering experiments - are labelled by S and P, respectively. Because of the ^{54}Fe and ^{56}Fe contaminants in the ^{58}Fe targets, it was necessary to measure the ^{54}Fe(p,γ) and ^{56}Fe(p,γ) excitation curves to determine if these impurities constituted any serious background problem. The respective NaI(Tl) excitation curves are shown in Fig. 15. As can be seen, the yields are not very large (the ^{54}Fe and ^{56}Fe target thickness, 1 to 2 $\mu g/cm^2$, were comparable to the ^{58}Fe target thickness) and the level densities are much lower than in ^{59}Co.

Over the analogue state region (2.15 to 2.30 MeV) 22 Ge(Li) spectra were taken. A typical spectrum is shown in Fig. 16. As in Fig. 12, gamma rays corresponding to transitions which were most often observed have been labelled. Of these only the level at 1.292 MeV has been positively identified as being a $3/2^-$ state. The peak at about 800 keV is due to the inelastic decay. In Fig. 17 the absolute gamma decay widths for the 10 analogue state fragments are shown. These absolute widths, as well as those for the 12 s-waves, are tabulated in Appendix A. Estimates of the total gamma widths for the analogue state fragments were again made and have been included in Appendix A.

Figure 14. Elastic scattering and NaI(Tl) excitation curves over the ground state analogue in ^{59}Co. The S and P labels denote the $\ell = 0$ and $\ell = 1$ resonances as determined from the present elastic scattering experiments.

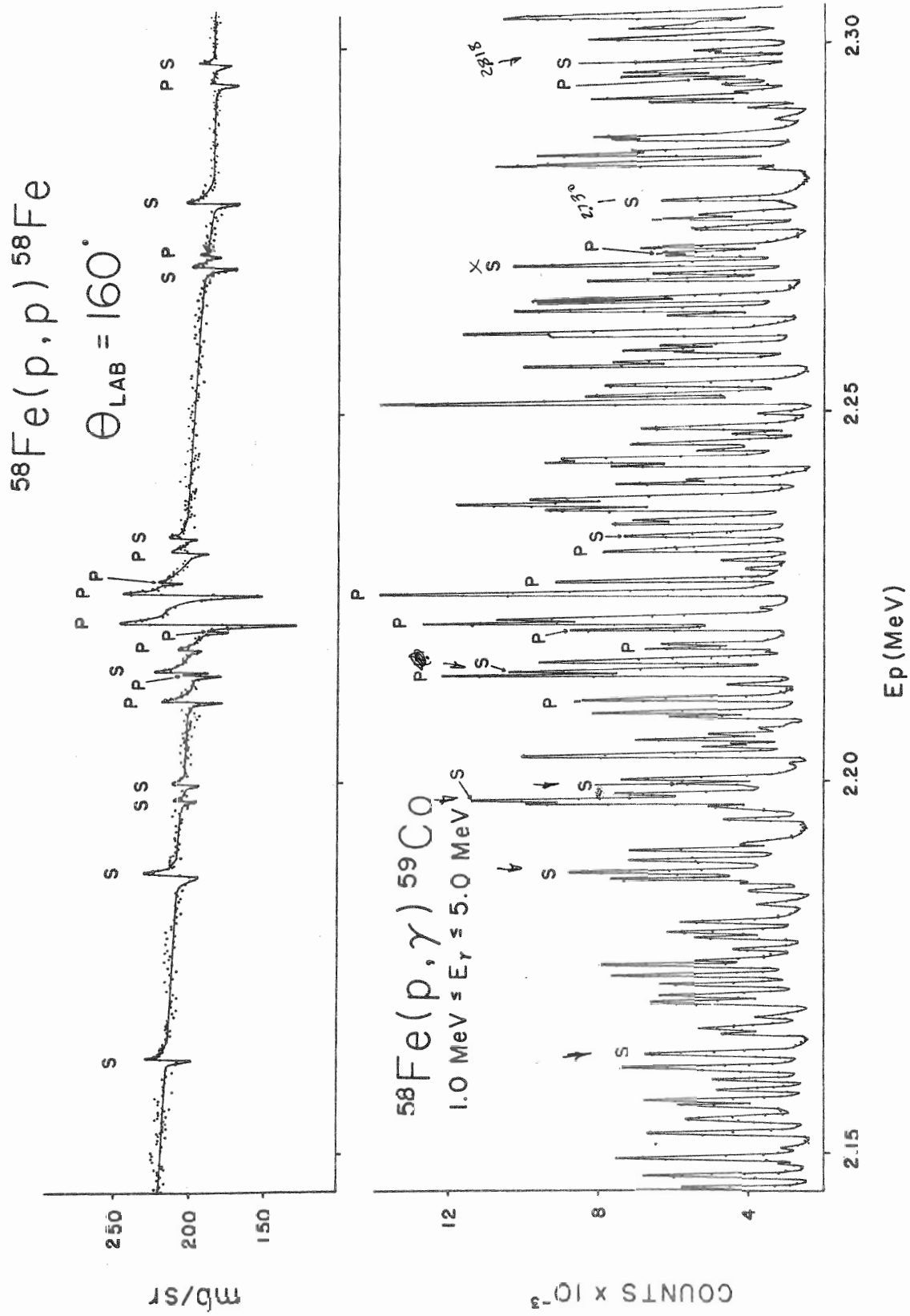
58Fe(p,p)58Fe
θLAB = 160°
mb/sr
250
200
150
S
S
S S
P P P
P S
P P
P
P
S P
S
P S
58Fe(p,γ)59Co
1.0 MeV ≤ Er ≤ 5.0 MeV
COUNTS x 10-3
12
8
4
2.15
2.20
2.25
2.30
Ep(MeV)
2818
273°
X

Figure 15. The $^{54}Fe(p,\gamma)$, $^{56}Fe(p,\gamma)$, and $^{58}Fe(p,\gamma)$ NaI(Tl) excitation curves over the region of the ^{59}Co ground state analogue.

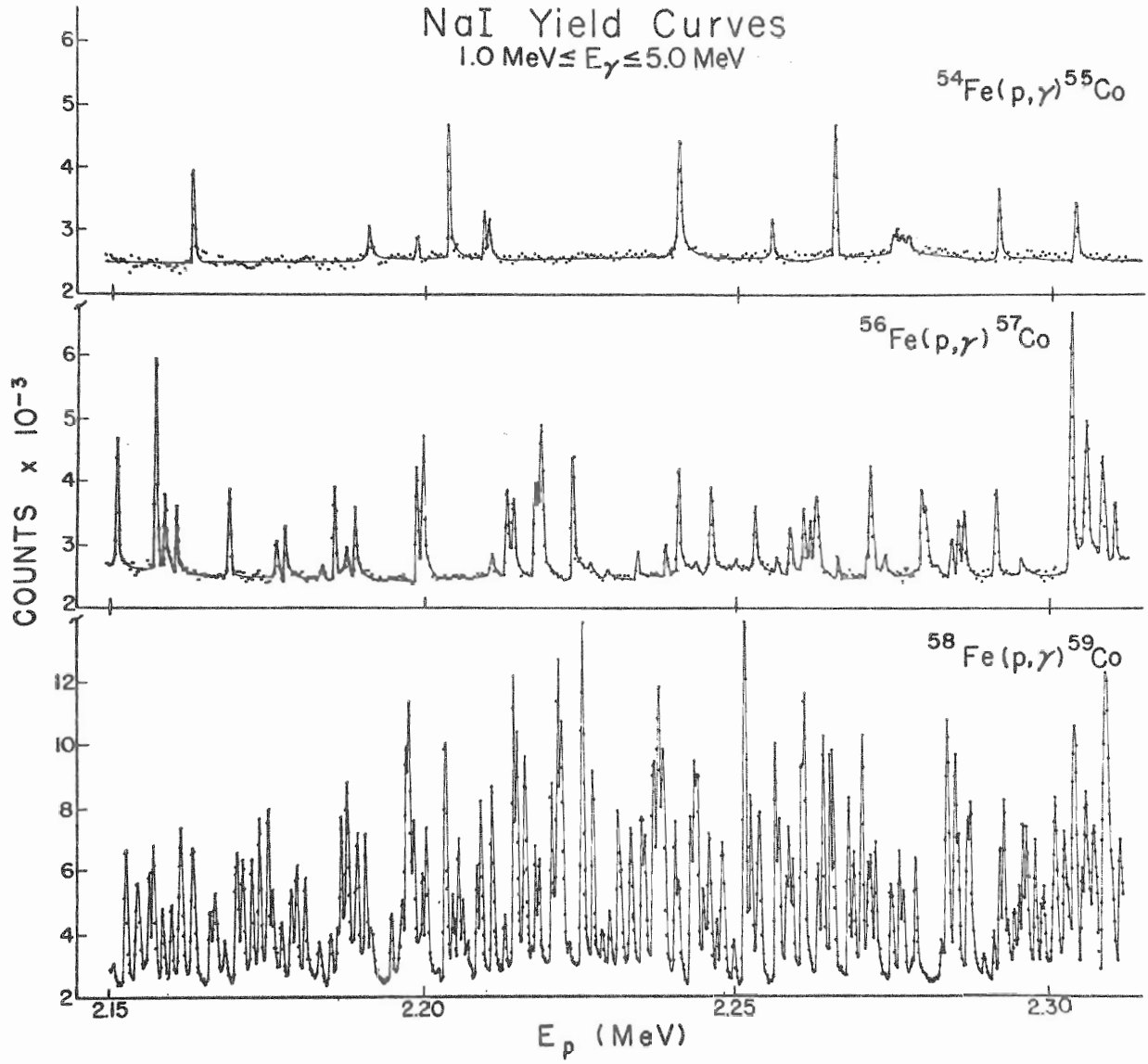
NaI Yield Curves
1.0 MeV≤ Eγ≤5.0 MeV
54Fe(p,γ)55Co
56Fe(p,γ)57Co
58Fe(p,γ)59Co
COUNTS x 10-3
Ep (MeV)
2.15
2.20
2.25
2.30

Figure 16. A typical $^{58}Fe(p,\gamma)^{59}Co$ Ge(Li) spectrum.

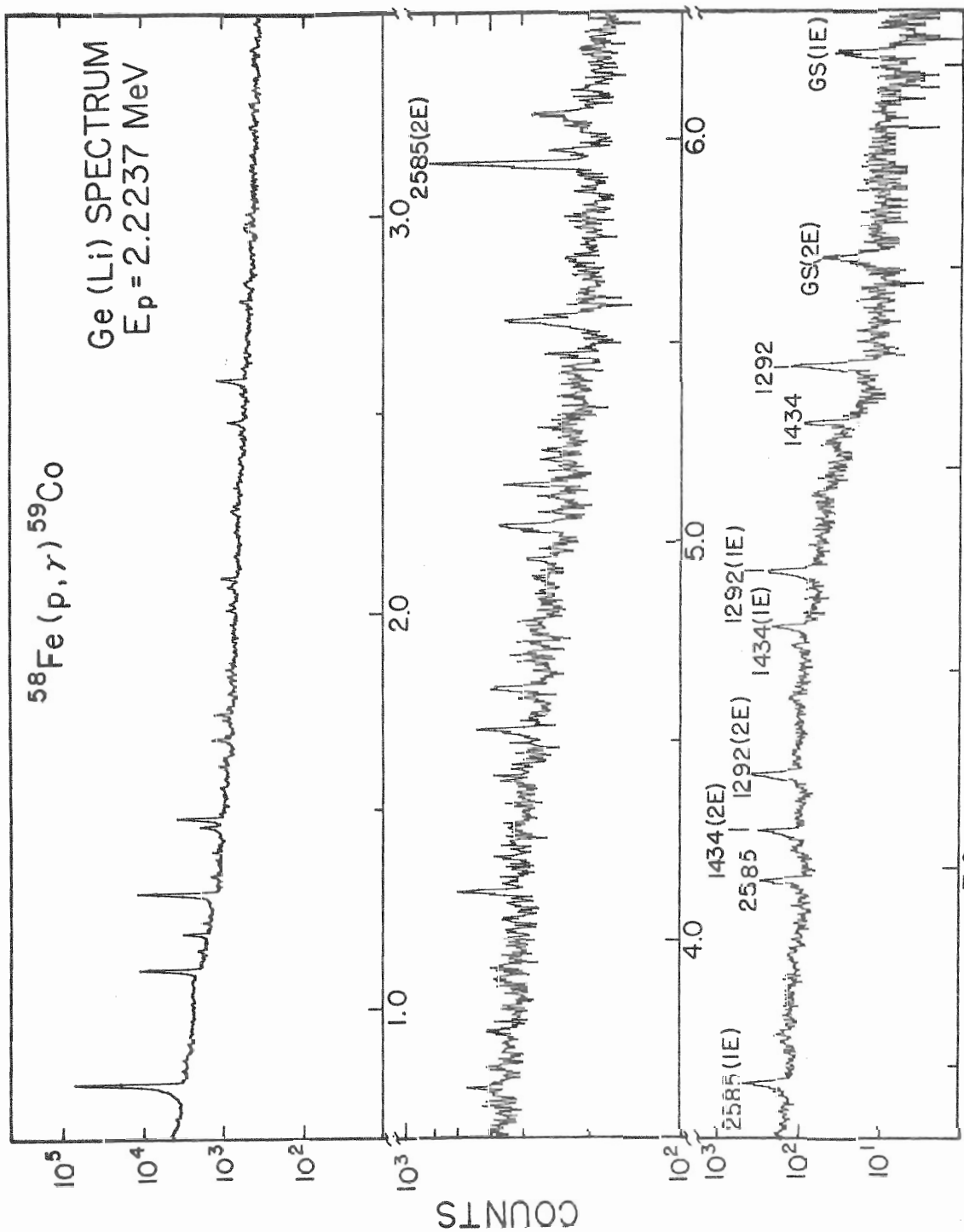
$^{58}Fe(p,\gamma)^{59}Co$
Ge (Li) SPECTRUM
$E_p = 2.2237$ MeV
COUNTS
E_γ (MeV)
2585(2E)
GS(2E)
GS(1E)
1292
1434
1292(1E)
1434(1E)
1292(2E)
1434(2E)
2585
2585(1E)

Figure 17. Absolute gamma decay widths for the fragments of the ground state analogue in ^{59}Co.

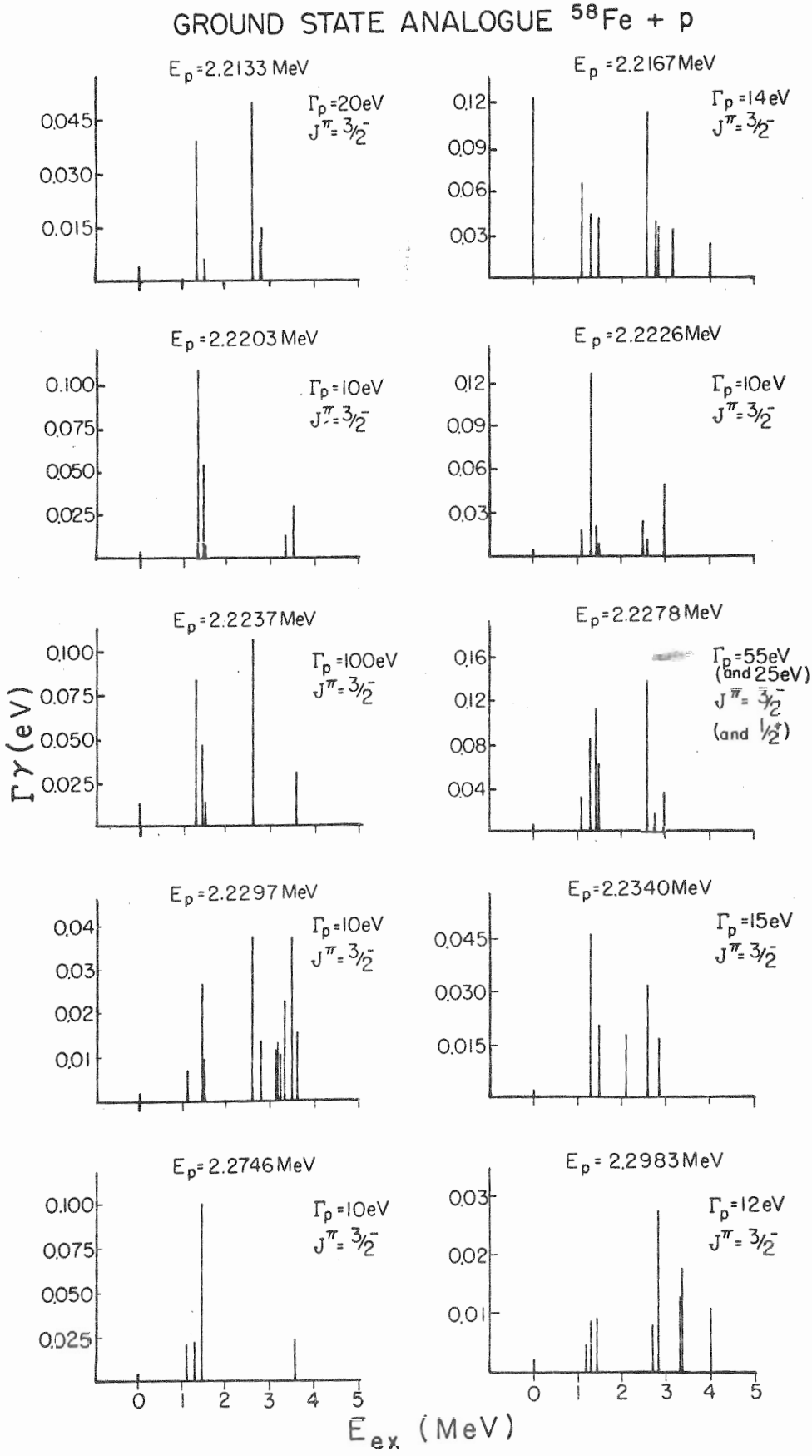
GROUND STATE ANALOGUE $^{58}Fe + p$
E_p=2.2133 MeV
Γ_p=20eV
$J^\pi = 3/2^-$
E_p=2.2167MeV
Γ_p=14eV
$J^\pi = 3/2^-$
E_p=2.2203 MeV
Γ_p=10eV
$J^\pi = 3/2^-$
E_p=2.2226MeV
Γ_p=10eV
$J^\pi = 3/2^-$
E_p=2.2237MeV
Γ_p=100eV
$J^\pi = 3/2^-$
E_p=2.2278MeV
Γ_p=55eV (and 25eV)
$J^\pi = 3/2^-$ (and $1/2^+$)
E_p=2.2297MeV
Γ_p=10eV
$J^\pi = 3/2^-$
E_p=2.2340MeV
Γ_p=15eV
$J^\pi = 3/2^-$
E_p=2.2746MeV
Γ_p=10eV
$J^\pi = 3/2^-$
E_p=2.2983MeV
Γ_p=12eV
$J^\pi = 3/2^-$
$\Gamma\gamma$ (eV)
E_{ex} (MeV)

Chapter V

ANALYSIS AND DISCUSSION

A. ^{55}Mn Ground State Analogue

The gamma decay patterns shown in Fig. 12 indicate that the fragments of the ground state analogue in ^{55}Mn do not decay the same way. Not only are the branching ratios different for each of the fragments, but the number of observed transitions and the gamma decay strengths (in eV) vary significantly from resonance to resonance. There are some distinct patterns in the decays, however. The decays of the fragments with the stronger elastic widths (those with Γ_p = 115-, 25-, 55-, and 65 eV) are similar in that they are fairly strong, spread out somewhat evenly over a rather large energy range and dominated by the ground state transitions. On the other hand, the decays of the fragments at 1.9929-, 2.0020-, and 2.0059 MeV (the decay patterns for the 1.9929 and 2.0059 MeV levels are remarkably similar) are quite weak with almost no ground state transitions and with most of the strength of the observed decays in transitions to levels between 1.5 and 3.0 MeV. The fragment at 1.9842 MeV is quite anomalous because of the strength of

the transitions from it and because of the relative strength of the ground state transition. There is also some similarity in the decays in the sense that several of the transitions to low-lying levels occur commonly in the gamma decay of all of the fragments. Some of the more important of these common decays are the transitions to the ground state and to the levels at 1.528-, 2.251-, 2.564-, and 3.045 MeV. The (^{3}He,d) spectroscopic strengths (from Cujec and Szoghy, 1969), which are shown in Table 7, are concentrated in these five levels.

Table 7. (^{3}He,d) Spectroscopic Strengths for Low-Lying States in ^{55}Mn

Excitation Energy (MeV)	J^π	$(2J+1)\,C^2S$
0.000	$5/2^-$	0.21
1.528	$3/2^-$	0.59
2.251	$3/2^-$	1.73
2.564	$(3/2)^-$	0.46
3.045	$(3/2)^-$	0.46

The M1 strengths (in Weisskopf units) for transitions to the four $\ell = 1$ states are shown in Table 8. These strengths have been determined by assuming that the E2/M1 mixing ratio is zero. The total strength of the transition to the level at 2.251 MeV (which has the largest (^{3}He,d) spectroscopic factor), 0.053 Wu, is in good agreement with the

Table 8. M1 Strengths for $\Delta J = 0$ Transitions from the Ground State Analogue in ^{55}Mn

	E_{final} (MeV)			
E_p (MeV)	1.528	2.251	2.564	3.045
1.9842	0.023	0.034	0.015	0.020
1.9875	0.004	0.000	0.008	0.015
1.9929	0.003	0.002	0.002	0.004
2.0020	0.002	0.004	0.003	0.019
2.0059	0.005	0.004	0.005	0.006
2.0075	0.001	0.004	0.001	0.001
2.0089	0.006	0.003	0.008	0.018
2.0113	0.000	0.002	0.002	0.000
Total	0.044	0.053	0.044	0.083

previous findings of inhibited IAS-AIAS M1 transitions in this mass region.

The beta decay of ^{55}Cr populates the five above-mentioned states in ^{55}Mn. The log ft values (from Hill, 1970) and gamma decay-beta decay comparisons for the transitions to these states are given in Table 9. The width Γ_β has been determined from the formula given in Chapter II, section C, for the beta decay "M1 transition strength". Γ_γ (eV) is the corresponding experimental gamma decay width summed over the 8 fragments. The gamma decay transition to the level at 2.368 MeV was not seen in the decays of the analogue state fragments. Thus an upper limit for this width is 8 (fragments) X 0.005 eV (the estimated level of observability) = 0.040 eV, as shown in Table 9. The poor agreement between Γ_β and Γ_γ is not unexpected for the 4 transitions for which Γ_β is small. When the beta decay is so weak, a slight admixture of $T_<$ states in the $T_>$ state could account for the large Γ_γ values. In the case of the decay to the ground state, however, the beta decay is probably too strong for this to account for the discrepancy. One possible explanation for the difference is that the E2/M1 mixing ratio for the ground state transition could be appreciable.

The gamma decay widths for the transitions to the ground state and to the levels at 2.251-, 2.564-, and 3.045 MeV are shown in Fig. 18 along with the elastic, inelastic, and total gamma widths (which, in this case, are the estimates from the primary transitions). There is some similarity between the patterns for the elastic, inelastic, and ground state

Table 9. Comparison of ^{55}Cr Beta Decay with the Gamma Decay of the Ground State Analogue in ^{55}Mn

E_{ex} (MeV) of Final State	J^{π}	Log ft	Γ_{β} (eV)	Γ_{γ} (eV)
0.000	$5/2^-$	5.0	0.38	1.43
1.528	$3/2^-$	6.9	0.0029	0.55
2.251	$3/2^-$	6.1	0.014	0.51
2.266	$(1/2)^-$	7.4	0.0007	0.21
2.368	$5/2^-$	6.2	0.011	0.04

Figure 18. Channel decay widths for the 8 fragments of the ground state analogue in ^{55}Mn.

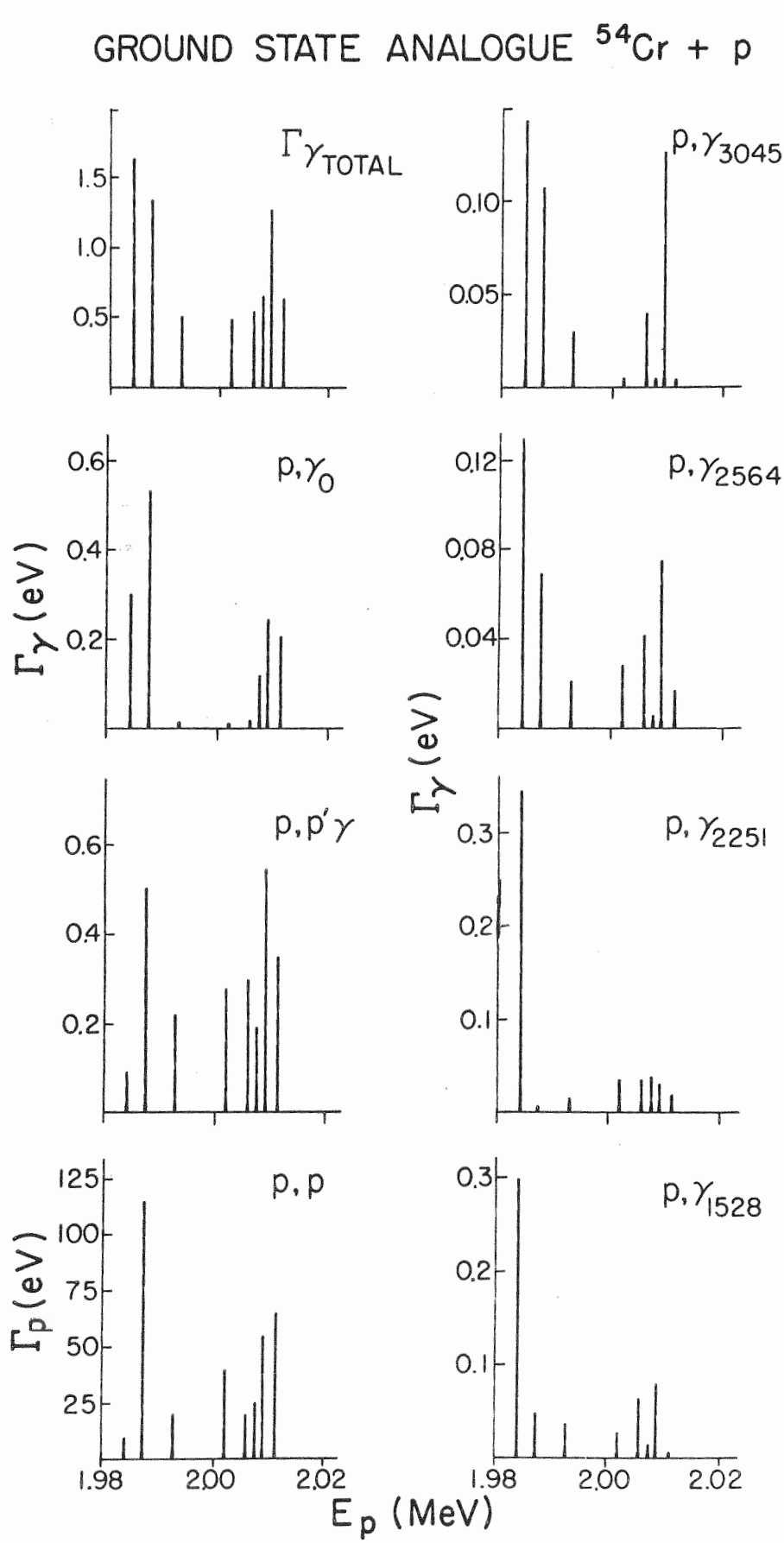
GROUND STATE ANALOGUE $^{54}Cr + p$
$\Gamma\gamma_{TOTAL}$
p,γ_{3045}
p,γ_0
p,γ_{2564}
$p,p'\gamma$
p,γ_{2251}
p,p
p,γ_{1528}
$\Gamma\gamma$ (eV)
Γ_p (eV)
E_p (MeV)
1.98
2.00
2.02

transitions. In Table 10 the linear correlation coefficients between each pair of the decay channels shown in Fig. 18 are given. The 95% ranges of the confidence factors for correlations with the elastic widths are -0.52 and 0.75 (that is, the probability of obtaining a LCC greater than -0.52, or less than 0.75, between the elastic widths and a set of 8 random widths from a Porter-Thomas distribution is 95%). For correlations between 2 sets of widths obeying a Porter-Thomas distribution, the 95% ranges are -0.59 to 0.63. From Table 10, then, the correlation between the elastic and inelastic widths is statistically significant (that is, greater than 95% confident). The correlation between the elastic and ground state channels is significant at a (confidence) level of 94%. Some of the other correlations are also quite strong, for example those between the decays to the levels at 1.528-, 2.251-, 2.564-, and 3.045 MeV. The explanation for these strong correlations is not clear.

B. ^{59}Co Ground State Analogue

From the gamma decay patterns shown in Fig. 17, it is clear that the fragments of the ground state analogue in ^{59}Co also do not decay the same. There are fewer similarities in these patterns than there were in those of the ^{55}Mn resonances. The decay of the ^{59}Co fragments are characterized by the smaller number of observed transitions to low-lying levels between 1 and 3 MeV and by the weakness of these

Table 10. Channel - Channel Correlations for the ^{55}Mn Ground State Analogue

	p,p	p,p'γ	p,γ_0	p,γ_{1528}	p,γ_{2251}	p,γ_{2564}	p,γ_{3045}	p,γ_{Total}
p,p	1	0.79	0.73	-0.37	-0.47	0.02	0.18	0.26
p,p'γ		1	0.45	-0.42	-0.61	0.00	0.25	0.16
p,γ_0			1	0.30	0.19	0.57	0.67	0.81
p,γ_{1528}				1	0.96	0.90	0.74	0.75
p,γ_{2251}					1	0.76	0.54	0.63
p,γ_{2564}						1	0.93	0.90
p,γ_{3045}							1	0.94

transitions (the width of the strongest observed transition from any of the ^{59}Co fragments is only 0.14 eV compared to 1.2 eV for the strongest transition from the ^{55}Mn fragments). Furthermore, there are no clear patterns which characterize more than two of the fragments. As in the ^{55}Mn case, however, the decay patterns have several transitions in common. However very little (^{3}He,d) work has been done on levels in ^{59}Co and hence it is difficult to determine which levels are fragments of the antianalogue state. Table 11 shows the known (^{3}He,d) spectroscopic strengths (from Blair and Armstrong, 1965) for levels in ^{59}Co.

Table 11. (^{3}He,d) Spectroscopic Strengths for Low-Lying Levels in ^{59}Co

Excitation Energy (MeV)	J^{π}	$(2J+1)C^2S$
0.000	$7/2^-$	1.36
1.099	$3/2^-$	0.44
1.292	$3/2^-$	1.36
1.434	$1/2^-$	0.74

The M1 strengths (in Wu) for transitions from the fragments to the $3/2^-$ states at 1.099 MeV and 1.292 MeV are given in Table 12. The transition to the level at 2.585 MeV has been included in this table because

Table 12. M1 Strengths for Transitions from the Ground State Analogue in ^{59}Co

E_p (MeV)	E_{final} (MeV)		
	1.099	1.292	2.585
2.2133	0.000	0.003	0.007
2.2167	0.005	0.004	0.016
2.2203	0.000	0.009	0.001
2.2226	0.002	0.011	0.002
2.2237	0.000	0.007	0.015
2.2280	0.003	0.007	0.019
2.2297	0.001	0.000	0.005
2.2340	0.000	0.004	0.004
2.2746	0.002	0.002	0.001
2.2983	0.000	0.001	0.001
Total	0.014	0.048	0.071

the widths associated with it were unusually large. However the spin for this level has not been established.

The beta decay of ^{59}Fe populates the four states whose (^{3}He,d) spectroscopic strengths are known. Beta decay-gamma decay comparisons for these levels are given in Table 13 (the log ft values have been taken from Vervier, 1968). Γ_{β} has been omitted for the ground state transition because it is not M1. Unfortunately the beta decay is too weak to draw any conclusions from the comparisons.

In Fig. 19 the channel decay widths for several of the gamma transitions are shown with the elastic, inelastic, and total gamma decay widths (in this case the estimate from the secondary transitions). There is again a similarity between the elastic and inelastic patterns. Linear correlation coefficients between the 9 sets of widths shown in Fig. 19 are given in Table 14. The 95% ranges for correlations with the elastic widths are -0.40 and 0.67. For correlations with widths obeying a Porter-Thomas distribution, the 95% ranges are -0.45 and 0.63. Thus the elastic-inelastic correlation is again statistically significant. Also significant are the correlations between the total gamma decay widths and the elastic and inelastic widths.

In the ^{59}Co experiments, absolute gamma decay widths were determined for 12 s-waves in the region of the analogue state. Table 15 shows the linear correlation coefficients between several channels for these states. The linear correlation coefficients in this table are con-

Table 13. Comparison of ^{59}Fe Beta Decay with the Gamma Decay of the Ground State Analogue in ^{59}Co

E_{ex} (MeV) of Final State	J^{π}	log ft	Γ_{β} (eV)	Γ_{γ} (eV)
0.000	$7/2^-$	10.9	------	0.16
1.099	$3/2^-$	6.7	0.0046	0.14
1.292	$3/2^-$	5.9	0.027	0.57
1.434	$1/2^-$	6.5	0.0065	0.39

Figure 19. Channel decay widths for the 10 fragments of the ground state analogue in ^{59}Co.

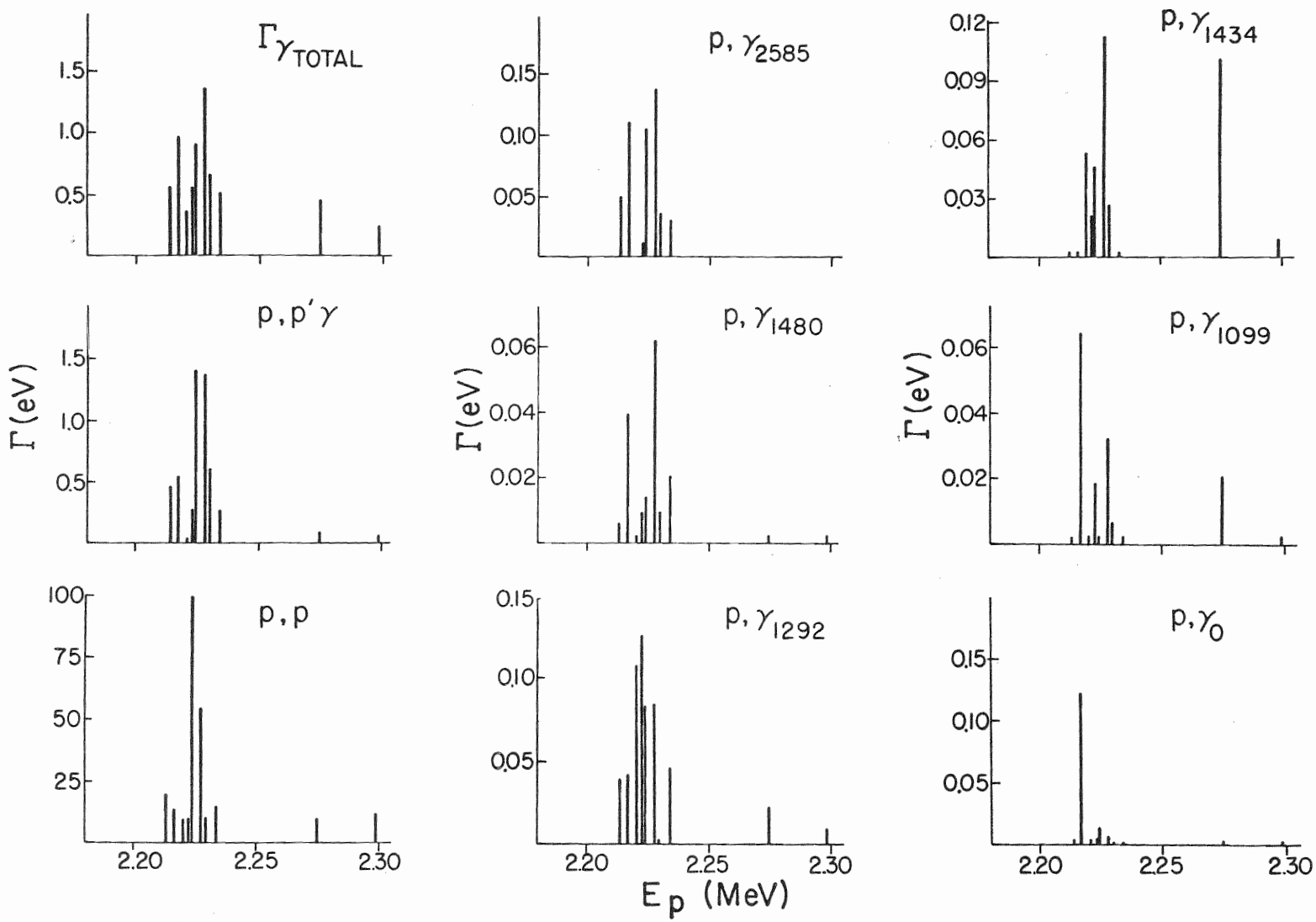
GROUND STATE ANALOGUE $^{58}Fe + p$
$\Gamma_{\gamma_{TOTAL}}$
p, γ_{2585}
p, γ_{1434}
p, p' γ
p, γ_{1480}
p, γ_{1099}
p, p
p, γ_{1292}
p, γ_0
Γ (eV)
Γ (eV)
Γ (eV)
1.5
1.0
0.5
0.15
0.10
0.05
0.12
0.09
0.06
0.03
1.5
1.0
0.5
0.06
0.04
0.02
0.06
0.04
0.02
100
75
50
25
0.15
0.10
0.05
0.15
0.10
0.05
2.20
2.25
2.30
2.20
2.25
2.30
2.20
2.25
2.30
E_p (MeV)

Table 14. Channel - Channel Correlations for the ^{59}Co Ground State Analogue

	p,p	p,p'γ	p,γ_0	p,γ_{1099}	p,γ_{1292}	p,γ_{1434}	p,γ_{1480}	p,γ_{2585}	p,γ_{Total}
p,p	1	0.88	-0.05	-0.09	0.30	0.32	0.35	0.67	0.60
p,p'γ		1	0.09	0.18	0.22	0.34	0.66	0.88	0.87
p,γ_0			1	0.84	-0.06	-0.29	0.43	0.48	0.39
p,γ_{1099}				1	0.03	0.13	0.65	0.52	0.58
p,γ_{1292}					1	0.21	0.19	0.15	0.24
p,γ_{1434}						1	0.28	0.19	0.38
p,γ_{1480}							1	0.86	0.91
p,γ_{2585}								1	0.95

Table 15. Channel - Channel Correlations for s-Waves in the Region of the Ground State Analogue in ^{59}Co

	p,p	p,p'γ	p,γ_{1099}	p,γ_{1292}	p,γ_{Total}
p,p	1	0.35	-0.026	-0.11	0.00
p,p'γ		1	-0.35	-0.14	-0.11
p,γ_{1099}			1	-0.29	0.00
p,γ_{1292}				1	0.81

sistent with purely statistical results expected of widths obeying a Porter-Thomas distribution. In particular, the total gamma widths are not correlated with the elastic or inelastic widths. The confidence factors are in the range of 50% to 60% for both the 0.00 and -0.11 linear correlation coefficients.

C. Conclusions

On the basis of the results presented in section A and B of this chapter, the status of correlations between fine structure widths in various channels for analogue states can be tentatively summarized:

1. there is evidence for correlations between the elastic and inelastic widths for the ground state analogues in ^{55}Mn and ^{59}Co

2. in the case of ^{55}Mn there is a correlation between the elastic and capture widths for the enhanced ground state transition corresponding to the strong Gamow-Teller beta transition from the parent state
3. few or no correlations have been observed between elastic and capture widths corresponding to antianalogue transitions from the ground state analogues in ^{55}Mn and ^{59}Co (these transitions are weak, in agreement with the results of previous experiments in this mass region)
4. the ^{59}Co elastic and total capture widths are correlated.

The strong correlations between the elastic and inelastic widths agrees with results found for a highly fragmented $3/2^-$ analogue state in ^{49}V (Prochnow, 1971). In the ^{49}V experiments, the inelastic widths were determined from inelastic proton yields by fitting the elastic and inelastic data simultaneously with the multilevel, multichannel R-matrix code normally used in the elastic scattering experiments. Prochnow determined the linear correlation coefficient between the elastic and inelastic widths (for 9 fragments) to be greater than 0.88 with a confidence factor of greater than 98%. He also showed that a correlation of elastic and inelastic widths for $3/2^-$ states off the analogue yielded a linear correlation coefficient of -0.17. Since the present experiments also show a strong correlation between the elastic and inelastic widths, it seems reasonable

to assume that for analogue state decay the correlation between the elastic and inelastic widths is now experimentally established. This correlation may be taken to indicate the enhancement of the inelastic widths, even though there is only slight evidence for the background strength of the inelastic scattering.

There is also evidence from other sources for correlations between the elastic and total capture widths, specifically, in fragmented analogue states in ^{47}Sc (Vingiani et al., 1971A) and ^{49}Sc (Vingiani et al., 1968B). Although these two analogue states are not as fragmented as the ^{55}Mn and ^{59}Co ground state analogues (the ^{47}Sc analogue has 6 fragments, the ^{49}Sc has 5), the correlations are still quite impressive. Using the widths given by Vingiani and Ricci (1971B), the linear correlation coefficients for both ^{47}Sc and ^{49}Sc are greater than 0.97 with a confidence level of greater than 98%. It is not clear what enhancement is implied by the elastic-total capture correlations for the analogue states in the two Sc isotopes and in ^{59}Co (expecially since no off-analogue data is available). The significant difference between the total capture width estimates for the ^{59}Co fragments that were made from the primary and secondary transitions (given in Table 17) suggests strong transitions to high energy states (4 to 7 MeV). The correlation between the elastic and total capture widths in ^{59}Co is presumably due to these transitions.

Chapter VI

SUMMARY

The electromagnetic decay of the $3/2^-$ ground state analogues in ^{55}Mn and ^{59}Co was studied with a 7.6 cm by 7.6 cm NaI(Tl) detector and an 80 cm^3 Ge(Li) detector. The NaI(Tl) detector was used to measure the $^{58}Fe(p,\gamma)^{59}Co$, $^{56}Fe(p,\gamma)^{57}Co$, and $^{54}Fe(p,\gamma^{55}Co$ excitation curves from E_p = 2.10 to 2.30 MeV and the $^{54}Cr(p,\gamma)^{55}Mn$ excitation curve from 1.98 to 2.02 MeV. These excitation curves were taken simultaneously with proton elastic scattering data so that the elastic scattering and capture resonances could be related. The proton energy resolution for the NaI(Tl) excitation curves was on the order of 300 to 350 eV. Using the NaI(Tl) detector to locate the resonances, Ge(Li) spectra were taken at the resonant energy of 10 resonances in the region of the ground state analogue in ^{55}Mn and of 22 resonances in the region of the ground state analogue in ^{59}Co. Analysis of elastic scattering data revealed that 8 of the 10 resonances in ^{55}Mn were fragments of the analogue (that is, $3/2^-$ states), and 10 of the 22 resonances in ^{59}Co were analogue state fragments.

The remaining resonances were all $1/2^+$. From the Ge(Li) spectra, absolute gamma decay and inelastic proton widths were determined for each of the resonances. Analysis of the capture data was limited by the efficiency of the Ge(Li) detector and knowledge of the level schemes in ^{55}Mn and ^{59}Co to transitions to low-lying states whose energies were less than about 3 MeV.

The strengths of the IAS-AIAS transitions in ^{55}Mn and ^{59}Co agree with results from the studies of unfragmented analogue states in this mass region. Specifically, the widths of these transitions are small, with the transitions to the states having the largest (^{3}He,d) spectroscopic factors being on the order of 0.05 Weisskopf units. Comparisons of several of the gamma decay widths with the beta decay of the parent states were made. In general the beta decay was too weak to allow a reasonable comparison. However the beta decay of ^{55}Cr to the ground state of ^{55}Mn was strong enough and led to an expectation of about 0.4 eV for the gamma decay width of the ground state transition. The experimental result for this width was 1.4 eV.

Linear correlation coefficients were determined between the decay widths for several channels for both of the fragmented analogue states. Included in these were the elastic, inelastic, partial gamma decay and total capture widths. The total capture widths were estimated from the primary transitions from the analogue state fragments and also from secondary transitions from low-lying levels to the ground states. Strong correlations

were found between the elastic and inelastic widths for both the ^{55}Mn and ^{59}Fe analogue states. From these correlations it was inferred that the inelastic widths are enhanced by the analogue state. The ground state transition in ^{55}Mn was found to be correlated with the elastic and inelastic widths. The explanation for these correlations was presumed to be the strong beta decay of ^{55}Cr to the ground state of ^{55}Mn. In ^{59}Co, the total capture widths (estimated from secondary transitions) were found to be highly correlated with the elastic and inelastic widths; but the reason for these correlations is not clear.

These experiments have definitely established the existence of correlations between the elastic and inelastic scattering widths for analogue states, and they have given tentative evidence for unexpected correlations between elastic and capture widths.

APPENDIX

Appendix A

The gamma decay widths determined from the Ge(Li) spectra are tabulated in this appendix. The resonant energies, E_p, are the laboratory energies of the incident proton beam. All widths are given in eV. The gamma decay transitions have been identified by the energy of the final states (in keV), which are given at the top of the tables. For the ^{55}Mn (Table 16) and ^{59}Co (Table 17) data, the gamma decay widths for transitions to levels whose excitation energies are greater than about 3.0 MeV are at best tentative because of the limitations of the Ge(Li) detector system and the uncertainty in the level schemes at such high excitation energies. The estimated uncertainty in the gamma decay and inelastic widths is 30% for widths greater than 0.05 eV, 50% for widths between 0.05 to 0.01 eV, and 100% for widths less than 0.01 eV. Where no transition has been observed (and left blank in Tables 16 and 17) the widths are estimated to be less than 0.005 eV. Γ_{Total} and Γ'_{Total} are the estimates of the total capture widths from the primary and secondary transitions, respectively.

Table 16. ^{55}Mn Resonance Widths

E_p	J^π	Γ_p	$\Gamma_{p'}$	Γ_{Total}	Γ'_{Total}
1.9777	$1/2^+$	13	0.026	1.85	**
1.9788	$1/2^+$	9	0.020	0.57	**
1.9842	$(3/2)^-$	10	0.092	1.62	1.63
1.9875	$3/2^-$	115	0.501	1.03	1.33
1.9929	$(3/2)^-$	20	0.218	0.25	0.50
2.0020	$3/2^-$	40	0.278	0.41	0.49
2.0059	$(3/2)^-$	20	0.297	0.43	0.54
2.0075	$(3/2)^-$	25	0.193	0.30	0.65
2.0089	$3/2^-$	55	0.545	1.07	1.25
2.0113	$3/2^-$	65	0.349	0.48	0.63

** Not estimated

Table 16. (continued)

E_p	Γ_{GS}	Γ_{126}	Γ_{1528}	Γ_{2251}	Γ_{2266}	Γ_{2425}
1.9777		0.023	1.290		0.054	
1.9788	0.051		0.024			0.045
1.9842	0.300	0.061	0.300	0.333	0.094	
1.9875	0.529		0.047			
1.9929	0.010		0.035	0.015		
2.0020	0.007	0.012	0.028	0.035		0.034
2.0059	0.018		0.064	0.036		
2.0075	0.119		0.015	0.038	0.017	
2.0089	0.242		0.080	0.032	0.084	
2.0113	0.206			0.020	0.017	0.030

Table 16. (continued)

E_p	Γ_{2564}	Γ_{2726}	Γ_{2751}	Γ_{2874}	Γ_{2950}	Γ_{2975}
1.9777						0.082
1.9788	0.034		0.066			0.103
1.9842	0.129	0.050	0.042	0.032		0.036
1.9875	0.069			0.068		0.017
1.9929	0.021		0.014			0.042
2.0020	0.028			0.048		
2.0059	0.042	0.032	0.014	0.054	0.042	
2.0075		0.063				
2.0089	0.074					
2.0113	0.016					

Table 16. (continued)

E_p	Γ_{3004}	Γ_{3037}	Γ_{3045}	Γ_{3050}	Other
1.9777		0.063			0.062(3081), 0.100(3429)
1.9788			0.180		0.024(3081), 0.048(3998)
1.9842					0.055(3505), 0.043(3883)
1.9875	0.061		0.107	0.027	0.029(4173), 0.078(4640)
1.9929	0.012	0.019	0.029		0.023(3425), 0.028(4110)
2.0020				0.134	0.046(3432), 0.036(4410)
2.0059	0.018		0.040		0.025(3385), 0.022(3611)
2.0075					0.019(3998), 0.019(4052)
2.0089			0.126		0.074(3081), 0.014(3195)
2.0113					0.060(4110), 0.050(4493)

Table 16. (continued)

E_p	Other (continued)
1.9777	0.034(3582), 0.055(4110), 0.088(4410)
1.9788	
1.9842	
1.9875	
1.9929	
2.0020	
2.0059	0.026(3752)
2.0075	0.020(4110), 0.024(5085), 0.034(5670)
2.0089	0.071(3385), 0.088(4110), 0.066(4493), 0.032(4638), 0.083(5667)
2.0113	0.039(4742), 0.039(4954)

Table 17. ^{59}Co Resonance Widths

E_p	J^π	Γ_p	$\Gamma_{p'}$	Γ_{Total}	Γ'_{Total}
2.1389	$1/2^+$	10	0.042	0.423	**
2.1513	$1/2^+$	7	0.041	0.462	**
2.1650	$1/2^+$	20	0.074	0.646	**
2.1745	$1/2^+$	10	0.081	0.542	**
2.1888	$1/2^+$	16	0.430	0.336	**
2.1896	$1/2^+$	21	0.214	0.633	**
2.1996	$(1/2^+)$	5	0.220	0.790	**
2.2020	$1/2^+$	12	0.339	0.303	**
2.2133	$(3/2)^-$	20	0.463	0.126	0.56
2.2167	$(3/2)^-$	14	0.538	0.510	0.98
2.2172	$1/2^+$	27	0.504	0.551	**
2.2203	$(3/2)^-$	10	0.038	0.213	0.37
2.2226	$(3/2)^-$	10	0.279	0.267	0.56
2.2237	$3/2^-$	100	1.406	0.295	0.92
2.2280*	$3/2^-$	55	1.366	0.491	1.36
2.2297	$(3/2)^-$	10	0.610	0.206	0.66
2.2340	$(3/2)^-$	15	0.269	0.136	0.51
2.2360	$1/2^+$	12	0.201	0.412	**
2.2730	$1/2^+$	20	1.291	0.493	**
2.2746	$(3/2)^-$	10	0.097	0.172	0.46
2.2818	$1/2^+$	25	0.112	0.460	**
2.2983	$(3/2)^-$	12	0.069	0.102	0.25

* Unresolved $1/2^+$, $3/2^-$ doublet.

** Not estimated

Table 17. (continued)

	E_p	Γ_{GS}	Γ_{1099}	Γ_{1190}	Γ_{1292}	Γ_{1434}	Γ_{1460}
	2.1389		0.370		0.015		
	2.1513		0.107		0.101	0.061	
	2.1650	0.003	0.167		0.082	0.184	
	2.1745	0.015	0.086		0.078	0.034	
	2.1888	0.008	0.008		0.034	0.018	
	2.1896	0.024			0.105	0.102	
	2.1996	(≤) 0.105	0.036		0.160		
	2.2020	0.009	0.012		0.047	0.022	
	2.2133	0.004			0.040		
	2.2167	0.123	0.064		0.042		
	2.2172	0.090	0.069		0.068	0.050	
	2.2203	0.004			0.107	0.054	0.005
	2.2226	0.005	0.019		0.126	0.021	
	2.2237	0.014			0.084	0.047	
	2.2280	0.007	0.032		0.085	0.112	
	2.2297	0.002	0.007			0.027	
	2.2340	0.002			0.046		
	2.2360		0.021		0.015	0.009	
	2.2730	0.010	0.024		0.060		
	2.2746	0.003	0.021		0.022	0.101	
	2.2818	0.005			0.085	0.224	
	2.2983	0.002		0.005	0.009	0.009	

Table 17. (continued)

E_p	Γ_{1481}	Γ_{1560}	Γ_{1744}	Γ_{2087}	Γ_{2206}	Γ_{2479}
2.1389						
2.1513	0.013					
2.1650						
2.1745						
2.1888		0.007		0.064		
2.1896	0.028					0.086
2.1996			0.052		0.148	
2.2020	0.028					
2.2133	0.006					
2.2167	0.040					
2.2172	0.038			0.028		
2.2203						
2.2226	0.010					0.025
2.2237	0.014					
2.2280	0.062					
2.2297	0.010					
2.2340	0.021			0.018		
2.2360	0.121					0.025
2.2730	0.026		0.190			
2.2746						
2.2818						
2.2983						

Table 17 (continued)

E_p	Γ_{2585}	Γ_{2720}	Γ_{2770}	Γ_{2781}	Γ_{2826}	Γ_{2957}
2.1389					0.028	0.010
2.1513		0.026		0.060	0.024	0.021
2.1650						0.024
2.1745				0.053	0.044	0.064
2.1888			0.099			
2.1896			0.068		0.083	
2.1996				0.043		0.034
2.2020	0.070		0.038			0.022
2.2133	0.050		0.011	0.015		
2.2167	0.111		0.039		0.035	
2.2172	0.080				0.038	
2.2203						
2.2226	0.012					
2.2237	0.106					
2.2280	0.138		0.017			
2.2297	0.037			0.014		
2.2340	0.032				0.017	
2.2360		0.034				
2.2730					0.066	
2.2746						
2.2818		0.266	0.020		0.057	
2.2983		0.008			0.028	

Table 17. (continued)

E_p	Γ_{2967}	Other
2.1389		
2.1513		0.051(3249)
2.1650	0.030	0.033(3130), 0.019(3263), 0.044(3800), 0.031(3998), 0.030(4180)
2.1745	0.045	0.028(3325), 0.021(3370), 0.048(3590), 0.026(4820)
2.1888		0.034(3130), 0.031(3325), 0.034(3860)
2.1896		0.071(3160), 0.066(3998)
2.1996	0.025	0.102(3089), 0.086(3113)
2.2020	0.022	0.018(3160), 0.014(3194)
2.2133		
2.2167		0.033(3143), 0.022(3994)
2.2172		0.033(3122), 0.056(3315)
2.2203		0.013(3320), 0.030(3490)
2.2226	0.050	
2.2237		0.030(3570)
2.2280	0.038	
2.2297		0.012(3122), 0.013(3160), 0.011(3222), 0.023(3320), 0.039(3488), 0.016(3620)
2.2340		0.060(3240), 0.024(3350), 0.042(3650)
2.2360	0.062	0.051(3620), 0.067(3650)
2.2730		
2.2746		0.024(3580)
2.2818		0.044(4510)
2.2983		0.013(3345), 0.018(3365), 0.011(4005)

Appendix B

In order to measure absolute inelastic and gamma decay widths, it was necessary to know the absolute efficiency of the 80 cm^3 Ge(Li) detector for gamma rays whose energies ranged from about 0.8 MeV to 10.5 MeV. The method used to measure this efficiency curve was to determine the relative efficiency of the detector from about 600 keV to 10.8 MeV and then measure the absolute efficiency at one point on the relative efficiency curve. Below 5 MeV the relative efficiency was determined by using ^{56}Co and ^{66}Ga sources. The branching ratios for these sources have been taken from Camp and Meredith (1971). Since no sources with gamma rays above 5 MeV were available, the reaction $^{27}Al(p,\gamma)^{28}Si$ was used to obtain the high energy calibration points. Table 18 lists the reasonances that were observed and the reference from which the branching ratios were taken. All of these resonances decay strongly either to the first excited state in ^{28}Si at 1.780 MeV or to the third excited state at 4.617 MeV and hence provide relative efficiency calibration points which can be related to those from the ^{56}Co and ^{66}Ga sources. The high energy gamma rays from the

$^{27}Al(p,\gamma)^{28}Si$ resonances also provided data for the detector efficiency of the second escape peak. This data was processed in the form of the ratio of the second escape to the photopeak efficiencies.

Table 18. $^{27}Al(p,\gamma)^{28}Si$ Resonances used in the Relative Efficiency Measurements

E_p (keV)	Reference
992	Azuma et al. (1966)
1381	Meyer et al. (1969)
1388	Meyer et al. (1969)
2522	Antoufiev et al. (1964B)

The absolute efficiency of the Ge(Li) detector was determined from a calibrated ^{22}Na source (Lamaze, 1971). This source emits a strong 1.275 MeV gamma ray. In order to check the absolute efficiency curve, the total capture width of the E_p = 992 keV $^{27}Al(p,\gamma)^{28}Si$ resonance was measured from the yield of a thick target (22 keV at this resonance). The equation for the thick target absolute width has been given in Chapter III. The width obtained for this resonance was 24 ± 5 eV, in good agreement with the 22.8 ± 2.5 eV result measured by Lyons et al. (1969).

The absolute efficiency and second escape/photopeak ratio curves were parameterized by least square fitting polynomials of order up to 9 to the calibration points. For the absolute efficiency curve, the best results, that is the smallest chi-square, were obtained by fitting the logarithm of the efficiency with a cubic from 0.60 to 3.7 MeV and a quadratic from 3.7 to 10.5 MeV. A slight correction was required to smooth out the fit at 3.7 MeV. The estimated uncertainty in this parameterization of the efficiency curve is 10 to 15%. The absolute efficiency curve obtained from the polynomial fit is shown in Fig. 20 along with the second (double) escape efficiency curve. The double escape efficiency curve was obtained from a fit of a fifth order polynomial to the second escape/photopeak ratios and then multiplying by the photopeak absolute efficiency. The estimated uncertainty in the second escape/photopeak curve is 30%. In Tables 19 and 20 the Fortran computer subroutines which calculate the absolute efficiency, EFF (E) (where E is the energy of the full energy peak in keV) and the second escape/photopeak ratios, SEPP(E), are given. The results shown in Fig. 20 are in good qualitative agreement with those for a 50 cm^3 Ge(Li) detector which were obtained by Young et al. (1971). Also measured, but not shown in Fig. 20, was the ratio of the second escape to the first escape efficiencies. Within experimental error, this ratio was about 1.4 and independent of gamma ray energy.

The method for determining absolute gamma decay widths has been discussed in Chapter III. Not discussed, however, was the question

Figure 20. Photopeak and double escape absolute efficiencies for the 80 cm^3 Ge(Li) detector.

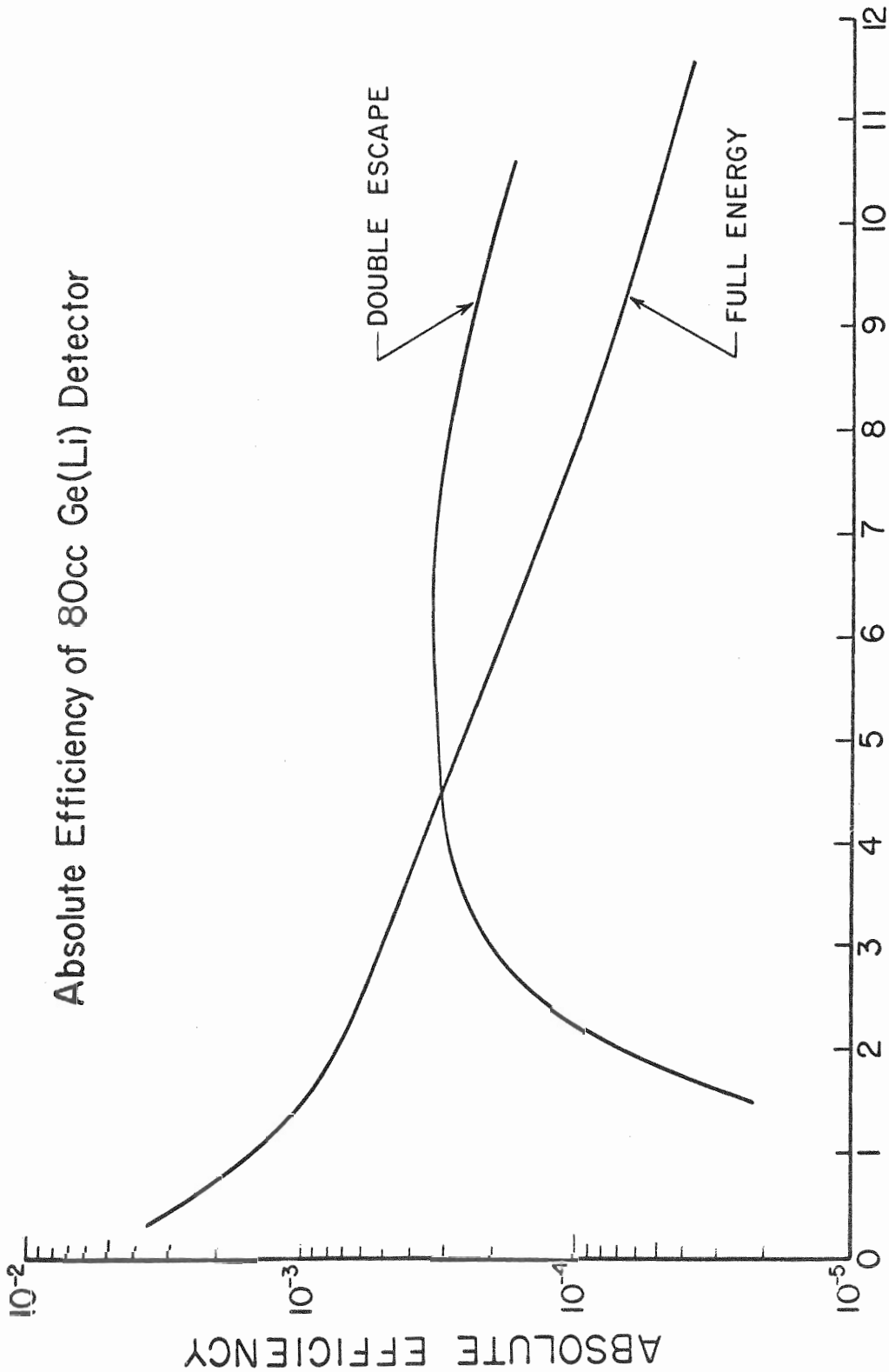
Absolute Efficiency of 80cc Ge(Li) Detector
DOUBLE ESCAPE
FULL ENERGY
ABSOLUTE EFFICIENCY
GAMMA RAY ENERGY (MeV)
10-2
10-3
10-4
10-5
0
1
2
3
4
5
6
7
8
9
10
11
12

Table 19. Listing of Subroutin EFF(E)

```
      FUNCTION EFF(E)
      DIMENSION A(9)
      DOUBLE PRECISION A, D, EN, T
      A(1) =  0.3324232D 01
      A(2) = -0.2043074D-02
      A(3) =  0.4699188D-06
      A(4) =  0.3811979D 01
      A(5) = -0.8881673D-02
      A(6) =  0.3036856D-04
      A(7) = -0.5584270D-07
      A(8) =  0.4687096D-10
      A(9) = -0.1455402D-13
      D    =  E/10.0
      T    =  D
      IF (E - 3710.0) 2, 1, 1
    1 CONTINUE
      EN =  A(1)
      N1 =  2
      N2 =  3
      GO TO 3
    2 CONTINUE
      EN =  A(4)
      N1 =  5
      N2 =  9
    3 CONTINUE
      DO 4 I = N1, N2
      EN = EN + A(I)*D
      D = D*I
    4 CONTINUE
      EFF =  EN
      EFF =  EFF - 6.00
      EFF =  10.00*EFF
      IF (E - 3000.0) 10, 10, 5
    5 CONTINUE
      IF (E - 3000.0) 6, 10, 10
    6 CONTINUE
      EFF = EFF*(1.00 - 0.42*EXP ((371.0 - E/10.0)*(E/10.0 -
                                                    371.0)/1936.0))
   10 CONTINUE
      RETURN
      END
```

Table 20. Listing of Subroutine SEPP(E)

```
      FUNCTION SEPP(E)
      DIMENSION A(6)
      DOUBLE PRECISION A, D, T. EF
      A(1) = 0.5725498D 00
      A(2) = 0.1941718D-01
      A(3) =-0.6643547D-04
      A(4) = 0.1203997D-06
      A(5) =-0.1059030D-09
      A(6) = 0.3515738D-13
      D = (E - 1022.0)/10.0
      T = D
      EF= A(1)
      DO 1 I = 2, 6
      EF = EF + A(I)*D
      D = D*T
1     CONTINUE
      SEPP = EF - 0.300D 01
      SEPP = 10.0**SEPP
      IF (E - 4200.0) 10, 10, 2
2     CONTINUE
      IF (E - 7800.0) 3, 10, 10
3     CONTINUE
      F = (6000.0 - E)/980.0
      F = F*F
      SEPP = SEPP*(1.00 + 0.090*EXP(-F))
10    CONTINUE
      RETURN
      END
```

of how a given peak in the Ge(Li) spectra was identified with a given transition (other than the procedure for determining the energy). For high energy gamma rays, $E_\gamma > 6$ MeV, this identification was facilitated by the appearance of single and double escape peaks. However, as shown in Fig. 20, the second escape/photopeak ratio is about 1 in the range of 4 to 5 MeV. So in this energy range the appearance of a single peak, with no clear escape peaks, made identification very difficult. In general, any gamma ray widths listed in Tables 16 and 17 which correspond to these energies should be considered tentative.

Appendix C

A. Chi-Squared Distributions

As presented by Porter and Thomas (1956), the chi-squared distribution for ν degrees of freedom is

$$P(x, \nu) = \frac{\frac{\nu}{2}\left(\frac{\nu x}{2}\right)^{\frac{\nu}{2}-1} \mathrm{Exp}(-\nu x/2)}{\Gamma(\nu/2)}$$

where $\Gamma(\nu/2)$ is the Gamma function. These distributions for several values of ν are shown in Fig. 21, which has been taken from Porter and Thomas (1956). For $\nu = 1$ the chi-squared distribution is identical to the Porter-Thomas distribution

$$P(x) = \mathrm{Exp}(-x/2)/\sqrt{2\pi x}$$

where $x = \gamma^2 / \bar{\gamma}^2$. This distribution characterizes the statistical fluctuation of nuclear reaction widths. If the average reduced widths for N decay channels are equal, the expected statistical distribution obeyed by the total reduced width, $\gamma^2 = \sum_{i=1}^{N} \gamma_i^2$, is the chi-squared distribution of N degrees of freedom.

Figure 21. The chi-squared distribution for several degrees of freedom.

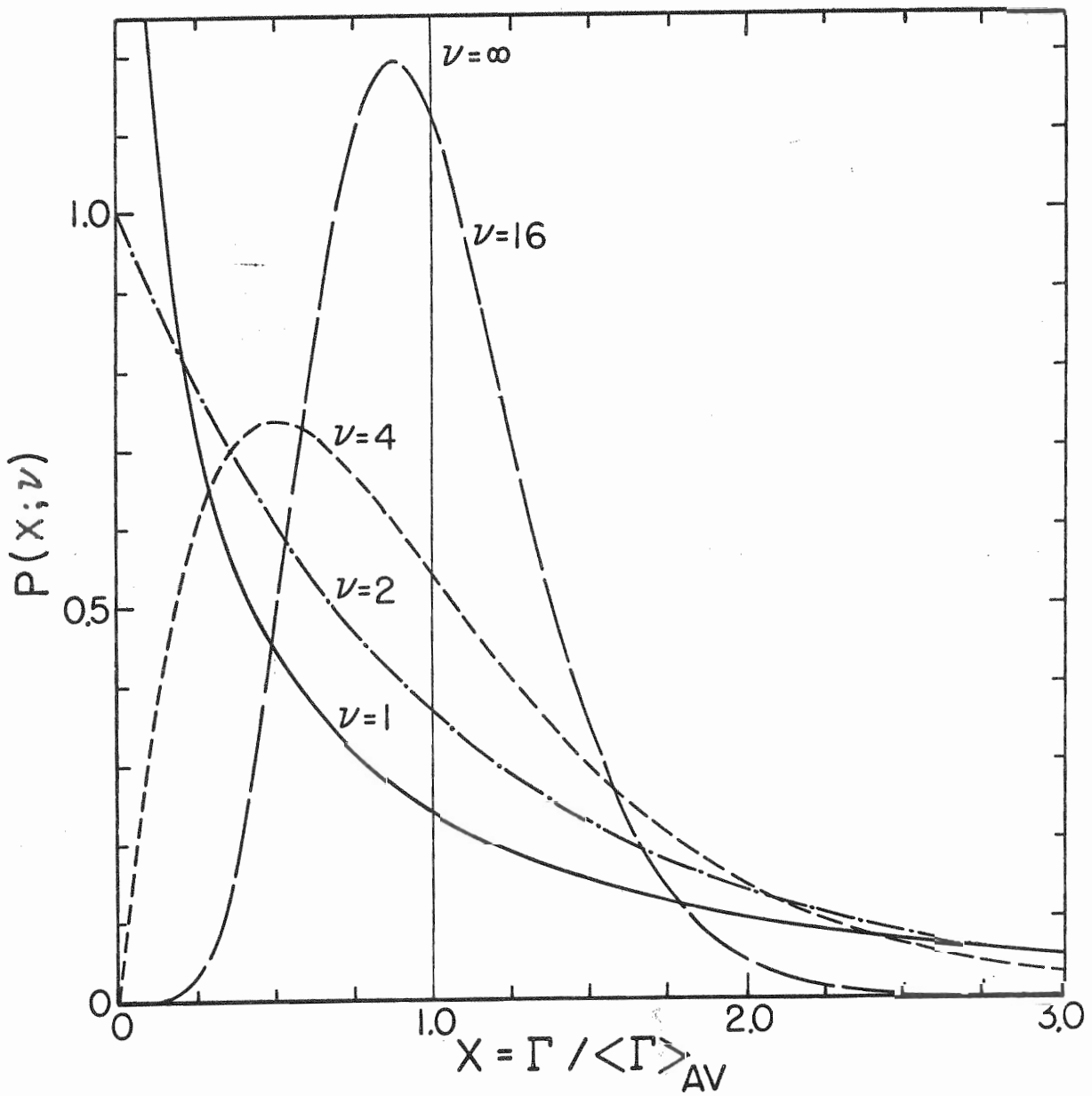
ν=∞
ν=16
ν=4
ν=2
ν=1
P(X;ν)
1.0
0.5
0
0
1.0
2.0
3.0
X = Γ / <Γ>AV

B. Method of Computer Generation of Random Numbers

The method used to generate random numbers from, say, a Porter - Thomas distribution required random numbers uniformly distributed from 0.00 to 1.00. These "uniform random numbers" were computer-generated by the Power Residue Method (IBM, 1969). For binary computers whose word size is $m = 2^b$, the procedure is the following:

> Choose any odd integer I_o for a starting value and choose an integer J of the form $J = 8T + 3$ (where T is any integer) for a multiplier. Calculate $I_{n+1} = J * I_n \pmod{2^b}$ using fixed point integer arithmetic, but interpret the result as a binary fraction. This fraction is then the desired random number. (IBM, 1969).

For best results J, the multiplier, should be approximately the square root of the computer word size, m. For example, the maximum word size for the DDP-224 computer is 8388608 ($=2^{23}$) so J was taken to be 2899. An important feature of the Power Residue Method is that the procedure can produce 2^{b-2} terms before repeating. For the DDP-224 computer this limitation is about 2.096 million random numbers.

C. Generation of Random Numbers from a Non-Uniform Distribution

In order to generate random numbers from the Porter - Thomas

and chi-squared distributions an acceptance-rejection method was used. As given by Zelen and Severo (1964), the procedure for this method is the following:

1. Assume a finite domain (a,b) for the distribution P(x). If the domain is infinite, a finite subset must be chosen for computational purposes.
2. Let $\bar{P}$ be the maximum value of P(x) on (a,b).
3. Generate a pair of random numbers, r and s, from a uniform distribution (described in section B).
4. Let $x_o = a + (b - a) * s$.
5. If $r < P(x_o)/\bar{P}$, then choose x_o as the random number. Otherwise reject r and s and start again.

The acceptance ratio for random numbers generated by this method is $\left[(b - a)\bar{P}\right]^{-1}$.

For the Porter-Thomas distribution, $\bar{P}$ is infinite so the acceptance-rejection method cannot be used directly. However by generating random numbers from a Gaussian distribution, Porter-Thomas random numbers can be obtained, since the squares of the Gaussian random numbers are distributed according to the Porter-Thomas distribution.

D. Confidence Factors

Confidence factors have been briefly discussed in Chapter III.

Typical results are shown in Fig. 22, which is the histogram obtained from the generation of 1000 linear correlation coefficients between sets of 8 Porter-Thomas random numbers. The acceptance ratio for the generation of these numbers (with a = 0.00, b = 10.0) was about 12%. Therefore approximately 256,000 random numbers uniformly distributed from 0 to 1 were generated, well below the 2.096 million allowed before repetition.

Figure 22. Histogram for correlations between sets of random numbers obeying the Porter-Thomas distribution.

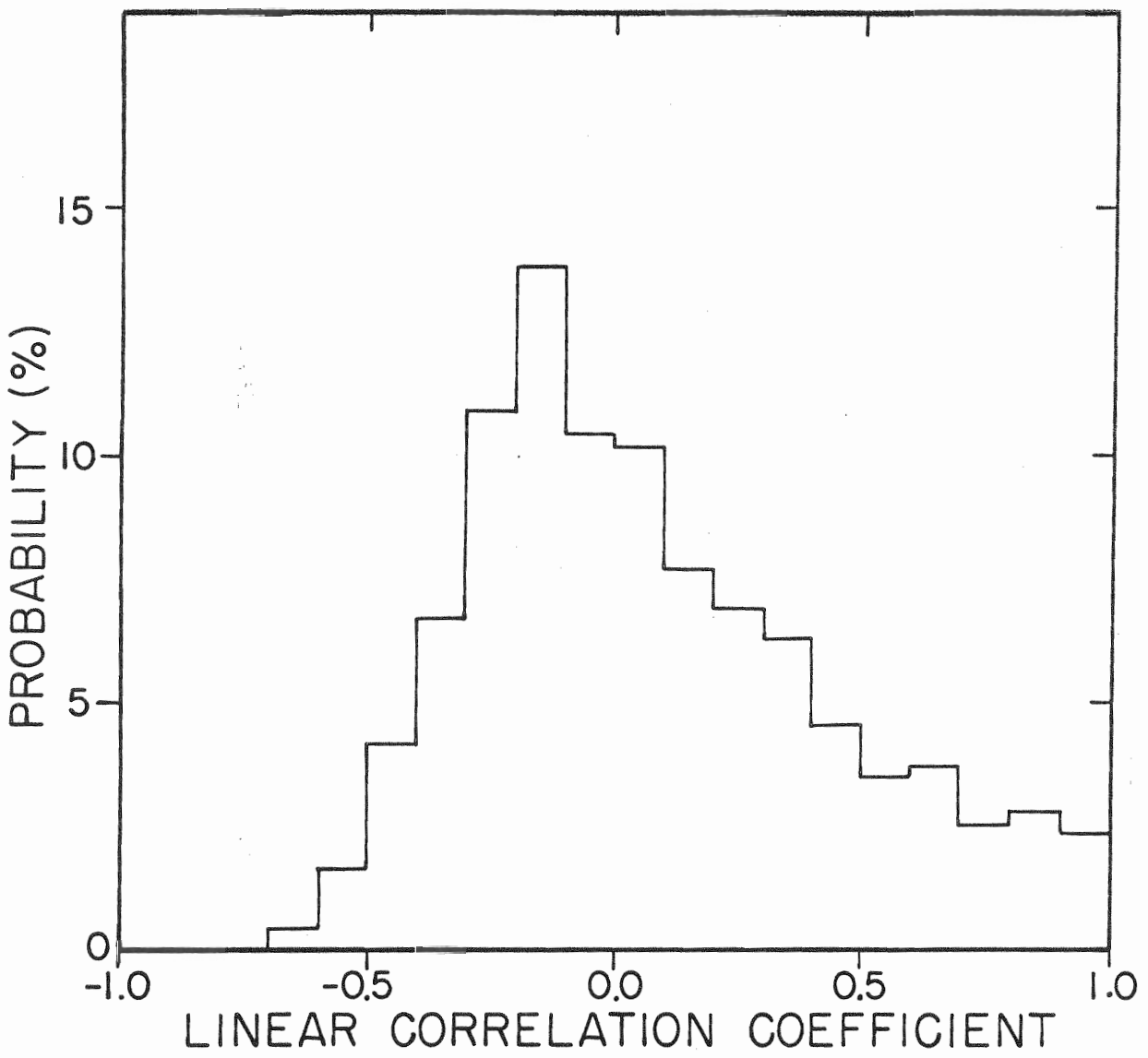
15
10
5
0
PROBABILITY (%)
-1.0
-0.5
0.0
0.5
1.0
LINEAR CORRELATION COEFFICIENT

Appendix D

In order to keep the 3 MV Van de Graaff laboratory electrical ground separated from that of the DDP-224 computer, commercially available optical isolators were used. Figure 23 shows a diagram of the circuit in which these isolators were employed. The optical isolators consists of a photodiode-phototransistor package. When a negative 3 to 10V signal appears at the input, as shown in the circuit diagram, the input transistor (2N3906) turns on the photodiode. Light picked up by the phototransistor sends current through the 4.7 K resistor on the output side. Voltage across this resistor causes the 2N3906 output transistor to turn on and -6 Volts appears as shown in Fig. 23. For this circuit, V_1 and V_2 were both 10 V. The response time of the optical isolators requires an input pulse width of at least 30 μsec.

Figure 23. Diagram of the circuit used to isolate the laboratory and computer electrical grounds.

ISOLATION CIRCUIT

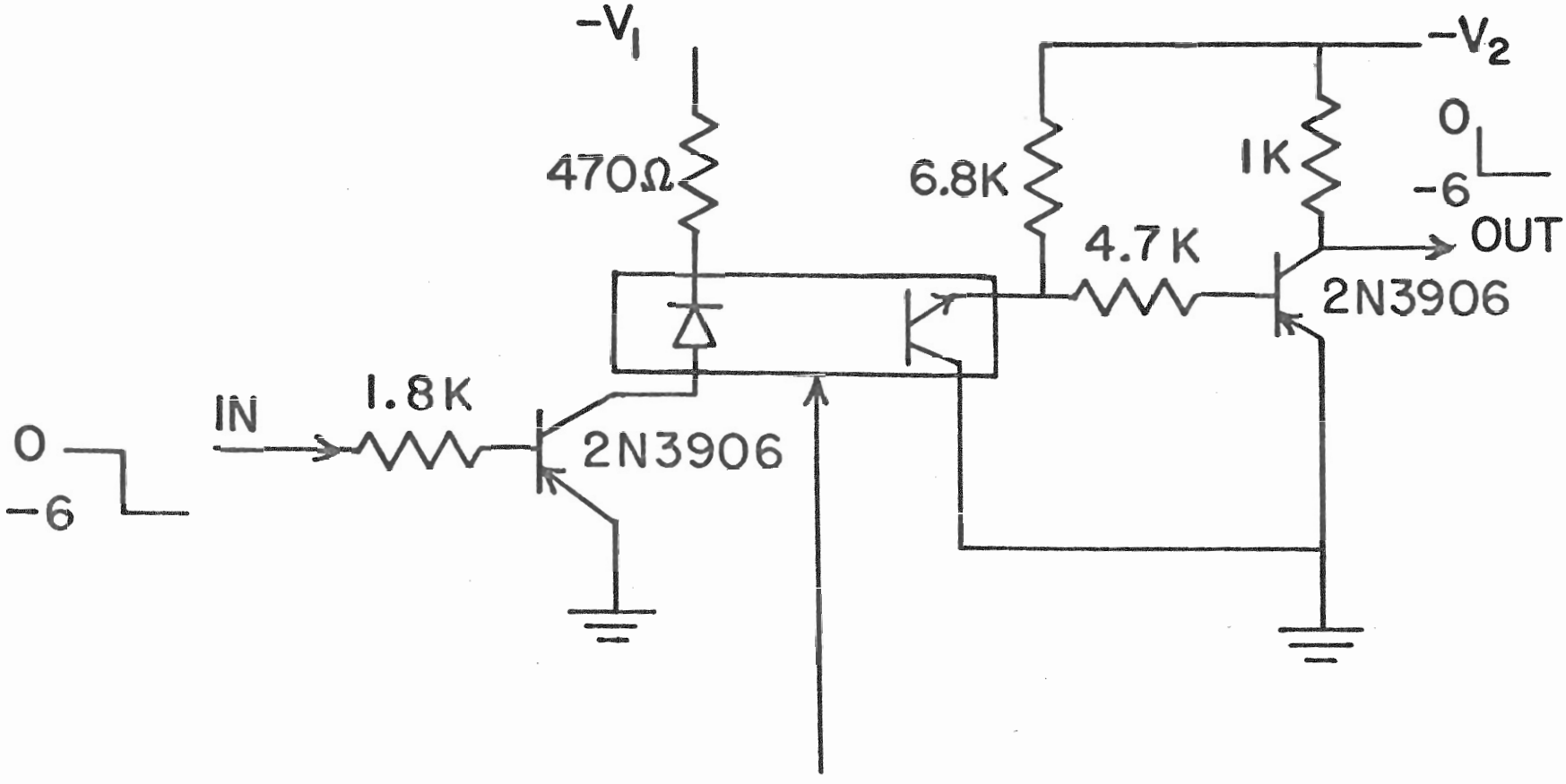

TIL107 OPTICAL ISOLATORS

LIST OF REFERENCES

LIST OF REFERENCES

E. G. Adelberger and D. P. Balamuth, Phys. Rev. Letters 27, 23 (1971) 1597.

F. Ajzenberg-Selove and T. Lauritsen, Nucl. Phys. 11 (1959) 1.

F. Ajzenberg-Selove and T. Lauritsen, Nucl. Phys. A114 (1968) 1.

Y. P. Antoufiev, L. M. El-Nadi, D. A. E. Darwish, O. E. Badawy and P. V. Sorokin, Nucl. Phys. 46 (1963) 1.

Y. P. Antoufiev, O. E. Badawy, L. M. El-Nadi, D. A. E. Darwish and P. V. Sorokin, Nucl. Phys. 54 (1964A) 301.

Y. P. Antoufiev, D. A. E. Darwish, O. E. Badawy, L. M. El-Nadi and P. V. Sorokin, Nucl. Phys. 56 (1964B) 401.

J. D. Anderson and C. Wong, Phys. Rev. Letters 7 (1961) 250.

J. D. Anderson and C. Wong, Phys. Rev. Letters 8 (1962 442.

J. D. Anderson, C. Wong and J. W. McClure, Phys. Rev. 126 (1962) 2170.

J. D. Anderson, C. Wong and J. W. McClure, Phys. Rev. 129 (1963) 2718.

R. L. Auble and J. Rapaport, Nucl. Data B3 - No. 3,4 (1970).

R. E. Azuma, L. E. Carlson, A. M. Charlesworth, K. P. Jackson, N. Aryas-Weiss and B. Lalovic, Can. J. Phys. 44 (1966) 3075.

W. H. Barkas and M. J. Berger, NAS-NRC Publication 1133, Nuclear Science Series, Report 39 (1964) 103.

P. R. Bevington, Data Reduction and Error Analysis for the Physical Sciences. (McGraw-Hill, New York, 1969).

A. G. Blair and D. D. Armstrong, Phys. Rev. 140 (1965) 1567.

J. M. Blatt and V. F. Weisskopf, Theoretical Nuclear Physics, (John Wiley and Sons, Inc., New York, 1952).

J. C. Browne, G. A. Keyworth, D. P. Lindstrom, H. W. Newson and E. G. Bilpuch, Phys. Letters 28B (1968) 26.

J. C. Browne, "Fine Structure of Analog States in ^{61}Cu, ^{63}Cu and ^{65}Cu," Unpublished Ph. D. dissertation, Duke University (1969).

D. C. Camp and G. L. Meredith, Nucl. Phys. A166 (1971) 349.

C. Chasman, K. W. Jones, R. A. Ristenen and J. T. Sample, Phys. Rev. Letters 18 (1967) 219.

G. Chilosi, R. A. Ricci and G. B. Vingiani, Phys. Rev. Letters 20 (1968) 159.

W. R. Coker and C. F. Moore, Phys. Today (1969) 53.

B. Cujec and I. M. Szoghy, Phys. Rev. 179 (1969) 1060.

P. M. Endt, "Second Symposium on the Structure of Low-Medium Mass Nuclei," ed. by P. Goldhammer and L. W. Seagondollar, (1966) 58.

P. M. Endt, Nuclear Structure, ed. by A. Hossain, et al., (Amsterdam, 1967) 58.

P. M. Endt, Third Symposium on the Structure of Low-Medium Mass Nuclei, ed. by J. P. Davidson, (University Press of Kansas, 1968) 73.

P. M. Endt, Nuclear Isospin, ed. by J. D. Anderson, S. D. Bloom, J. Cerny and W. W. True, (Academic Press, New York, 1969) 51.

F. C. Erne, W. A. M. Veltman and J. A. J. M. Wintermans, Nucl. Phys. 88 (1966) 1.

I. Fodor, I. Szentpetery and J. Szucs, Phys. Letters 32B (1970) 689.

J. D. Fox, et al., Phys. Rev. Letters 12 (1964) 198.

C. Gaarde, K. Kemp, Y. V. Naumov and P. R. Amundsen, Nucl. Phys. A143 (1970) 497.

H. E. Gove, Nuclear Reactions, Vol. I, ed. by P. M. Endt and M. Demeur, (North-Holland Publishing Company, Amsterdam, 1959) 302.

S. S. Hanna, Isospin in Nuclear Physics, ed. by D. H. Wilkinson, (North-Holland Publishing Company, Amsterdam 1969) 591.

G. I. Harris and J. J. Perizo, Phys. Rev. C 2 (1970) 1347.

J. C. Hill, Nucl. Phys. A150 (1970) 89.

M. Hirata, Phys. Letters 32B (1970) 656.

P. Holmberg and A. Kiuru, Com. Physico-Mathemiticae 40 (1970) 135.

IBM, Data Processing Techniques, "Random Number Generation and Testing," (1959).

G. A. Keyworth, "A High Resolution Study of Isobaric Analog States in ^{41}K and ^{23}Na," Unpublished Ph. D. dissertation, Duke University (1968).

G. A. Keyworth, G. C. Kyker, E. G. Bilpuch and H. W. Newson, Phys. Letters 20 (1966) 281.

G. A. Keyworth, G. C. Kyker, E. G. Bilpuch and H. W. Newson, Nuc. Phys. 89 (1966) 590.

H. V. Klapdor, Phys. Letters 35B (1971A) 405.

H. V. Klapdor, "Gamma Spectroscopy of T = 3/2 - 7/2 Analogue States of Nuclei in the f-p Shell," Unpublished Ph. D. dissertation, Max Planck Institute fur Kernphysik (1971B).

D. Kurath, Argonne National Laboratory Report 7108 (1965) 66.

G. P. Lamaze, Private correspondence (1971).

A. M. Lane, Isospin in Nuclear Physics, ed. by D. H. Wilkinson (North-Holland Publishing Company, Amsterdam, 1969) 509.

J. C. Legg, D. G. Megli, D. R. Abraham, L. D. Ellsworth and S. Hechtl, Phys. Rev. 186 (1969) 1138.

J. R. Leslie, W. McLatchie, C. F. Monahan and J. K. Thrasher, Nucl. Phys. A170 (1971A) 115.

J. R. Leslie, D. J. Martin and W. McLatchie, 36B (1971B) 76.

D. P. Lindstrom, "Fine Structure of Analog States in ^{55}Co, ^{57}Co, and ^{59}CO," Unpublished Ph. D. dissertation, Duke University (1970).

P. B. Lyons, J. W. Toevs and D. G. Sargood, Nucl. Phys. A130 (1969) 1.

M. H. Macfarlane and J. P. Shiffer, Comments on Nuclear and Particle Physics III (1969) 107.

L. G. Mann and S. D. Bloom, Nucl. Phys. A140 (1970) 598.

J. B. Marion, 1960 Nuclear Data Tables 3 NAS-NRC (1960) 160.

J. B. Marion and F. C. Young, Nuclear Reaction Analysis. (North-Holland Publishing Company, Amsterdam, 1968).

S. Maripuu, Nucl. Phys. A123 (1969) 357.

S. Maripuu, Nucl. Phys. A149 (1970A) 593.

S. Maripuu, Nucl. Phys. A153 (1970B) 183.

S. Maripuu, Phys. Letters 31B (1970C) 181.

S. Maripuu, J. C. Manthuruthil and C. P. Poirier, private communication (1972).

D. J. Martin, J. R. Leslie, W. McLatchie, C. F. Monahan and L. E. Carlson, Nucl. Phys. A187 (1972) 337.

M. A. Meyer and N. S. Wolmarans, Nucl. Phys. A136 (1969) 663.

M. A. Meyer, N. S. Wolmarans and D. Reitmann, Nucl. Phys. A144 (1970) 261.

J. N. Mo, B. Cujec, R. Dayras, I. M. Szoghy and M. Toulemonde, Nucl. Phys. A147 (1970) 129.

J. D. Moses, "A High Resolution Study of Isobaric Analog Resonances in ^{51}Mn, ^{53}Mn, and ^{55}Mn," Unpublished Ph. D. dissertation, Duke University (1970).

R. Nordhagen and A. Tveter, Nucl. Phys. 56 (1964) 337.

R. Nordhagen and A. Tveter, Nucl. Phys. 63 (1965) 529.

P. B. Parks, H. W. Newson and R. M. Williamson, Rev. Sci. Instr. 29 (1958) 834.

P. B. Parks, P. M. Beard, E. G. Bilpuch and H. W. Newson, Rev. Sci. Instr. 35 (1964) 549.

C. E. Porter and R. G. Thomas, Phys. Rev. 104 (1956) 483.

M. A. Preston, Physics of the Nucleus, (Addison-Wesley, Palo Alto, 1962).

N. H. Prochnow, "A High Resolution Study of Proton Resonances in ^{47}V, ^{49}V, and ^{51}V," Unpublished Ph. D. dissertation, Duke University (1971).

D. Robson, Phys. Rev. 137 (1964) 535.

D. Robson, Nuclear Isospin, ed. by J. D. Anderson, S. D. Bloom, J. Cerny and W. W. True, (Academic Press, New York, 1969) 385.

P. Richard, C. F. Moore, J. D. Fox and D. Robson, Phys. Rev. Letters 13 (1964) 343.

M. Sakai, R. Bertini and C. Gehringer, Nucl. Phys. A157 (1970) 113.

F. T. Seibel, Jr., "Neutron Resonances in ^{34}S, ^{40}A, and ^{48}Ca," Unpublished Ph. D. dissertation, Duke University (1968).

B. P. Singh and H. C. Evans, Nucl. Instr. and Meth. 97 (1971) 475.

I. Szentpetery and J. Szucs, Phys. Rev. Letters 28 (1972) 378.

I. Talmi and I. Unna, Annual Review of Nuclear Science, Vol. 10, ed. by E. Segre, G. Friedlander and W. E. Meyerhof (Annual Reviews, Inc., Palo Alto, 1960) 353.

J. Vervier, Nucl. Data B2 - No. 5 (1968).

G. B. Vingiani, R. A. Ricci, R. Giacomich and G. Poiani, Nuovo Cimento 57 (1968A) 453.

G. B. Vingiani, G. Chilosi and W. Bruyenstein, Phys. Letters 26B (1968B) 285.

G. B. Vingiani, G. Chilosi and C. Rossi-Alvarez, Phys. Letters 34B (1971A) 597.

G. B. Vingiani and R. A. Ricci, Topical Conference on the Structure of $1f_{7/2}$ Nuclei, ed. by R. A. Ricci, (Editrice Compositori-Bologna, 1971) 304.

J. Walinga, J. C. Manthuruthil and C. P. Poirier, Phys. Rev. 185 (1969) 1439.

E. K. Warburton, Isobaric Spin in Nuclear Physics, ed. by J. D. Fox and D. Robson, (Academic Press, New York, 1966) 90.

E. K. Warburton and J. Weneser, Isospin in Nuclear Physics, ed. by D. H. Wilkinson, (North-Holland, Amsterdam, 1969) 173.

D. D. Watson, J. C. Manthuruthil and F. D. Lee, Phys. Rev. 164 (1967) 1399.

W. M. Wilson, H. W. Newson, E. G. Bilpuch and G. E. Mitchell, Bull. Am. Phys. Soc. 17 (1972).

E. P. Wigner, Phys. Rev. 51 (1937) 106, 947.

F. C. Young, A. S. Figuera and G. Pfeufer, Nucl. Inst. and Meth. 92 (1971) 71.

M. Zelen and N. C. Severo, Handbook of Mathematical Functions with Formulas, Graphs, and Mathematical Tables, ed. by M. Abramowitz and I. A. Stegun, (U. S. Government Printing Office, Washington, 1964) 949.

BIOGRAPHY

William Carter Peters

Personal:	Born 25 January 1946, Richmond, Virginia
Education:	B. S., Physics and Mathematics, University of Richmond, 1967
Positions:	NDEA Fellow, Duke University, 1967-1970 Research Assistant, Duke University, 1970-present
Memberships:	American Physical Society
Publication:	Channel Correlation Effects for Fragmented Analog States (with G. E. Mitchell, E. G. Bilpuch, J. D. Moses and N. H. Prochnow). Statistical Properties of Nuclei, ed. by J. B. Garg (Plenum Press, New York, 1972) 299.
Abstract:	Gamma Decay of the Fine Structure of the Isobaric Analog of the Ground State of ^{55}Cr (with E. G. Bilpuch, G. E. Mitchell and G. L. Morgan). Bull. Am. Phys. Soc. 16 (1971).